SANDIA REPORT SAND82-0161 • Unlimited Release • UC-15
Printed September 1982

Far-Infrared Contraband-Detection-System Development for Personnel-Search Applications

Ralph L. Schellenbaum

Prepared by
Sandia National Laboratories
Albuquerque, New Mexico 87185 and Livermore, California 94550
for the United States Department of Energy
under Contract DE-AC04-76DP00789

SF 2900-Q(6-82)

DISCLAIMER

Issued by Sandia National Laboratories, operated for the United States Department of Energy by Sandia Corporation.

Printed in the United States of America
Available from
National Technical Information Service
U.S. Department of Commerce
5285 Port Royal Road
Springfield, VA 22161

NTIS price codes
Printed copy: A03
Microfiche copy: A01

PAGES 1 to 2

WERE INTENTIONALLY

LEFT BLANK

SAND--82-0161

DE83 001029

SAND82-0161
Unlimited Release
Printed September 1982

Distribution
Category UC-15

Far-Infrared Contraband-Detection-System Development for Personnel-Search Applications

Ralph L. Schellenbaum
Entry Control Systems Division 9252
Sandia National Laboratories
Albuquerque, NM 87185

Abstract

Experiments have been conducted toward the development of an active near-millimeter-wave, far infrared, personnel search system for the detection of contraband. These experiments employed a microwave hybrid tee interferometer/radiometer scanning system and "quasi-optical" techniques at 3.3-mm wavelength to illuminate and detect the reflection from target objects against a human body background. Clothing and other common concealing materials are transparent at this wavelength. Retroreflector arrays, in conjunction with a Gunn diode radiation source, were investigated to provide all-angle illumination and detection of specular reflections from unaligned and irregular-shaped objects. Results indicate that, under highly controlled search conditions, metal objects ≥ 25 cm^2 can be detected in an enclosure lined with retroreflectors. Further development is required to produce a practical personnel search system. The investigation and feasibility of alternate far infrared search techniques are presented.

Contents

Figures

Figures (cont)

Far Infrared Contraband Detection System Development for Personnel Search Applications

Introduction

Two of the goals of an effective entry control system are to detect the surreptitious introduction of contraband into a facility and prevent the unauthorized removal of special nuclear material. The contraband of most concern are weapons and explosives. The detection of shielding material that could be used to defeat the nuclear material detectors is also of concern. Currently, weapons and shielding detection are performed by screening personnel with a metal detector. One of the problems with this technique is that metal detectors will not find some of the composite materials that could be used to shield nuclear material. Explosives vapor detectors have been installed at nuclear plants licensed by the NRC. The available screening type vapor detectors are very limited in the population of explosive materials they can detect.

Scanning personnel with near-millimeter-wave (NMMW), far-infrared (FIR) radiation was proposed to overcome some of the difficulties of current screening methods. This spectral region (~300 to 3000 μm) is employed for personnel inspection because clothing and other common dielectric materials are nearly transparent and the low-level microwave radiation is biologically safe. The selected wavelengths of 1.4 and 3 mm (215 and 94 GHz) provide resolution on the order of 1 cm with a reasonable antenna aperture (10 to 100 cm).

In operation, a person is scanned by a sensitive radiometer operating in the NMMW portion of the spectrum. The measurements are displayed as an image on a TV monitor. A security officer looks at the image and if an anomalous pattern is detected, the subject is further searched to determine if the anomaly was caused by contraband or just innocent material. The image is produced by an optical scanning system which scans a two-dimensional search matrix (1 m^2) comprised of $\sim 10^4$ picture elements. The use of NMMW scanning for contraband detection has been investigated for the last several years. The next section reviews the search concepts studied and the results obtained from previous investigations. Briefly, it was learned that passive scanning is impractical because the low level of emission from the human body results in excessively long scan times. Active illumination of the subject reduces the scan time but with a point source of illumination the specular reflection from a contraband object is usually pointed away from the receiver. The present study, which is the subject of the body of this report, investigated all-angle illumination.

Previous Investigations

Previous investigations[1-8] of radiometric imaging in the far infrared (NMMW) spectral region sought to establish a practical method for searching personnel for concealed contraband. Transmission and reflection properties of pertinent materials were determined to demonstrate the feasibility of this method. The measurements utilized a CO_2 driven HCN laser source, a mechanical chopper, a sample holder and translator, and pyroelectric and cooled GaAs detectors. Transmission results indicated low attenuation for clothing and other common, nonconducting concealment materials. Reflectivity data was obtained for a human hand and various explosives in addition to common materials. A brief quantitative description of these results are given in Appendix A.

The simplest search concept involves the passive radiometric measurement and comparison of the radiation emitted by the human tissue background and target object. The human body is normally a few degrees above ambient room temperature; however, a second factor is even more significant. Two objects of different emissivities at the same absolute temperature can be distinguished by measuring their apparent temperature (or emissivity) difference with a radiometer. The emissivity of human tissue is close to unity at NMMW wavelengths and a radiometer will measure body temperature roughly 10° to 15°C above ambient

room temperature. Concealed metallic objects are revealed as regions of moderate-to-low emissivity (or temperature) against the high-emissivity background of human tissue. Concealed objects also shadow the radiation from the human tissue background and reflect ambient background into the radiometer.

Radiometric detection measurements and scanned images were obtained in the passive mode for metallic objects, nuclear shielding materials, explosives, and common clothing materials against a human torso background. Results indicate that metallic sheets of about 2 cm^2 were detectable with the passive radiometric laboratory system measurements. Composite nuclear shielding materials (lead-loaded plastics, paraffin, etc.) are difficult to detect because their characteristics are more similar to the tissue background and the contrast depends upon placement and contact with the subject. Explosives material is very difficult to detect for these reasons, unless, of course, it is packaged in a more easily detected material. Therefore, because both higher signal levels and lower scan times are required (see Appendix A), attention was directed from a passive to an active illumination approach to increase object-to-background contrast and reduce scan times.

With active illumination the image received is primarily dependent on the reflectivity of the objects. Concealed metal objects efficiently reflect the illumination into the radiometer and appear as bright areas (or dark areas for a cold source) against the human tissue background.

Preliminary investigations in the active mode employed liquid nitrogen-cooled Eccosorb in foam boxes as cold sources. A number of boxes were positioned in the foreground to illuminate the human body and target object. Ideally, the source of illumination should extend over the entire hemispherical foreground to ensure that any randomly oriented planar, or irregularly shaped, object will reflect into the detector.

Metal objects were easily detected provided they had a specular reflective surface of several cm^2 and were suitably illuminated. The incomplete cold-load illumination was marginal for detecting C-4 and TNT against an Eccosorb background. However, Detasheet, Tovex (water gel), and Iremite (water gel and aluminum) were detectable. The explosives did not contrast as well with the human body because parts of the body are as specularly reflective as the explosives. Composite nuclear shielding materials were readily detected against the human background. Samples of lead shot in neoprene, RTV, polyethylene, and plaster of paris were used in the tests. The results fall between those of metals and explosives.

Preliminary observations with coherent klystron illumination produced enhanced results (Appendix A). The targets were illuminated with 1.4- and 3-mm wavelength radiation from a horn antenna coaxial with the mirror system. The five explosive samples were clearly detectable against an Eccosorb background, but again, some human body surfaces appear as reflective as the explosives. Composite nuclear shielding was detected with relatively high contrast against Eccosorb and with somewhat less against a human body background.

It was concluded in the previous studies that feasibility had been demonstrated, but that serious difficulties exist in the development of a practical NMMW imaging system. Active illumination is required for search time tradeoff. Low reflectivity materials are very difficult, if not impossible, to detect against a body background with areas of comparable reflectivity. The signal-to-noise ratio cannot be improved by a simple increase in illumination intensity. Unaligned metal plate targets are specular reflectors and cannot be detected against a human body background. Nonplanar metal objects with the only very small portions aligned with the scanning system (e.g., a fine line for a cylinder or a small spot for a sphere) are also practically impossible to detect using point source illumination.

Illuminating the object from all angles, however, is a possible solution for objects of sufficiently high reflectivity. With this kind of illumination, the detector will receive the energy reflected from the entire cross section of the object with an effective increase in S/N ratio. A practical detection system will require the development of an all-angle bright source of uniform illumination, or the equivalent.

It also became apparent that, although coherent sources produce the more intense illumination required, they introduce new problems not easily solved. The problems are illuminating large areas from all angles, preventing excessive scattered background radiation from entering the detector, and eliminating interferometric effects.

The remainder of the present report describes the illumination experiments at SNL. Appendix B to this report describes the design of quasi-optical lens, polarizers, and beam splitters for use in the far infrared region. The intent is to document details which will aid in any future experimentation.

Experimental Procedure

Radiometric Imaging System

The brightness (B) of radiation emitted from a blackbody is governed by Planck's radiation law for a temperature (T) and radiation frequency (ν)

$$B = \frac{2h\nu^3}{c^2} \frac{1}{e^{h\nu/kT} - 1} \quad ,$$

where

B = brightness (W m^{-2} Hz^{-1} rad^{-2})
h = Planck's constant (6.63 x 10^{-34} j-s)
ν = frequency (Hz)
c = velocity of light (3 x 10^8 m s^{-1})
k = Boltzman's constant (1.38 x 10^{-23} j K^{-1})
T = temperature (K)

For nonideal blackbodies, emissivity $\epsilon \leq 1$ and the brightness follows the Stefan-Boltzman relation

$$B = \epsilon\sigma T^4 \quad ,$$

where

ϵ = emissivity = 1 for perfect blackbody
σ = constant (1.8 x 10^{-8} W m^{-2} K^{-4}) .

A Dicke radiometer was employed in the previous detector system.[14] In this method, a chopper alternately blocks the input signal and reflects a reference signal from an ambient load into the horn antenna. The signal is heterodyned, amplified, square-law detected, and synchronously detected in a lock-in amplifier. In the active mode, the chopper was eliminated by square-wave modulating the klystron. The system noise temperature (double sideband) is 30,000 K for the 1.4-mm radiometer and 1200 K for the 3-mm radiometer. The scanning system employed a fixed, elliptical, primary mirror and vertical and horizontal scanning mirrors.

The experiments reported here employed a microwave equivalent and radiometric variation of the Michelson interferometer.[9,10] This device is shown schematically in Figure 1. The same Schottky diode coherent detector is employed, but the chopper/lock-in amplifier synchronous detection is eliminated by a preset near-blackbody reference at ambient temperature. Figure 2 is a photograph of the detector/transmitter apparatus. The cylindrical object in the foreground is the collimating horn/lens receiver and transmitter antenna. Antireflection machining in the plastic lens can be seen as concentric grooves in the lens surface.

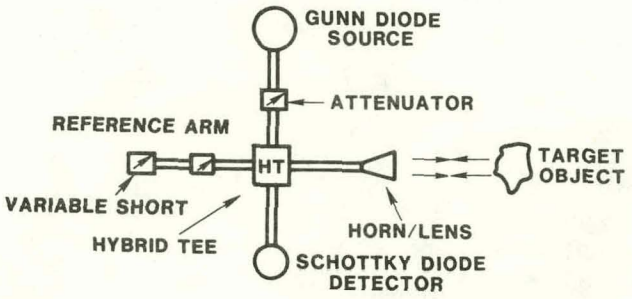

Figure 1. Hybrid Tee Interferometer/Radiometer Assembly

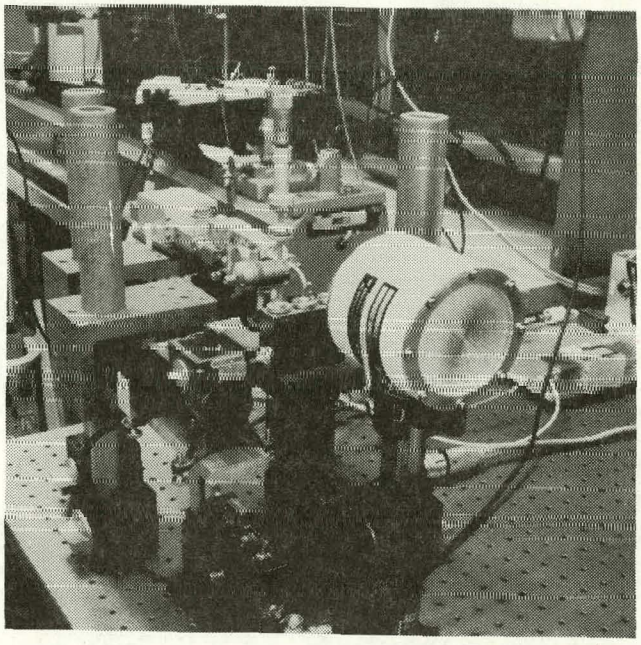

Figure 2. Hybrid Tee Radiometer Experimental Apparatus

The hybrid tee divides the radiation from the Gunn diode oscillator source (91 GHz, 20 mW) equally between the test arm and the reference arm. The target object reflects a signal back into the detector and, inconsequentially, into the oscillator arm. The variable short and attenuator in the reference arm control the phase and amplitude of the reflected signal into the detector. Small constant signals also enter the detector and form a part of the reference signal, e.g., hybrid-tee cross-leakage (~20 dB isolation) and reflections from imperfect horn antenna matching. Thus, detector output depends upon the phase relationship and amplitude of the two input signals and, when properly balanced as an interferometer, is very sensitive to target distance.

The hybrid tee system, however, can be operated in a radiometer mode in which the distance sensitivity and interference effects resulting from the use of coherent radiation are suppressed. By replacing the target with Eccosorb and nulling the Eccosorb background signal and the controllable reference signal for a given oscillator attenuator setting, the detector will respond mainly to beam intensity at signal levels above that of Eccosorb. The distance dependence was reduced 75% to 90%. It is not possible to perfectly control the reference signal because the backscattered radiation from the mirror system varies during scanning. Scanning directly with the detector assembly can improve imaging results. Eliminating the mirror system will reduce system backscattering and background interference effects.

The hybrid tee/collimating horn imaging system is suited to our application because it is simple to operate, it is compact for direct scanning, and the on-axis transmitter/receiver horn antenna is ideal for the collimated beam, retroreflecting-wall illumination method. Sensitivity and resolution with the 7.6-cm-dia horn/lens antenna is equal to or better than either the imaging mirror system with the 38-cm-dia primary mirror, Dicke radiometer, and 10-mW klystron, or the preliminary nonscanning, Cassegrain antenna-detector system. The hybrid tee system was chosen as the best radiometer for retroreflector experiments.

It may be noted, for completeness, that other techniques for eliminating or reducing coherence effects were briefly investigated. A linearly oscillating mirror was employed in the optical path of the nonscanning Cassegrain interferometric system to produce a $1/2\lambda$ cyclic shift in path length. Integrating the resultant signal output can yield an average value which is, ideally, independent of the target distance. This method was of interest for familiarization and proof of principle, but is not as advantageous as the hybrid tee radiometer method.

The present Imagining System is shown schematically in Figure 3. It consists of a mirror scanning system, hybrid tee illuminator/radiometer, electronics for scanning control and computer signal processing, and visual display and recording systems. The collimated search beam is scanned over an object plane of about 1 m^2 generating 10^4 picture elements. Radiation reflected from a suitably oriented object in the search plane is reflected back along the same path into the horn/lens antenna, hybrid tee, and Schottky diode detector. The detector and scanner control signals are processed by the Colorado video unit, displayed on a TV monitor, and stored in a Nova 3 computer.

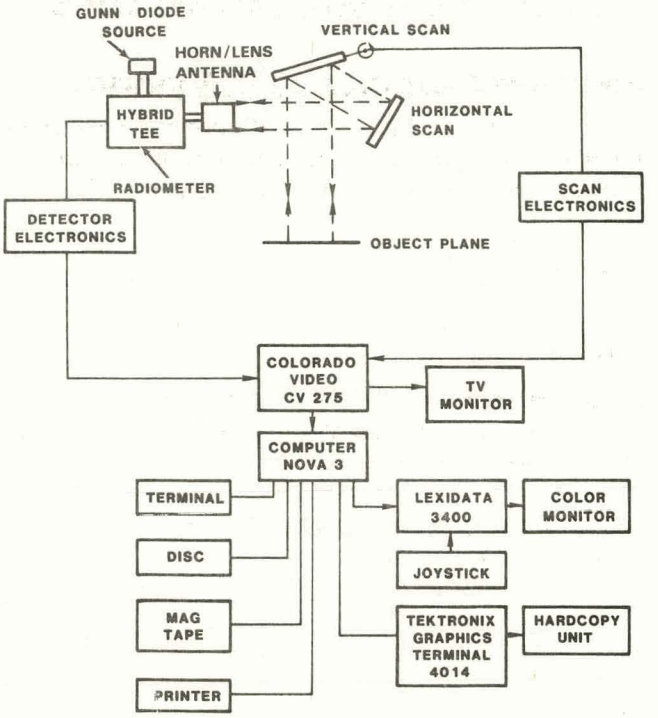

Figure 3. Imaging Detection System and Data Processing

Data analysis is performed using the joystick-controlled Lexidata 3400. Images are displayed on the color monitor in 63 shades of gray or color and can be zoomed to a single pixel. The joystick directs a cross-indicator to a pixel whose intensity and coordinate values are indicated in a graph below the image which includes all the pixels in the same horizontal scan. The same data can be displayed and printed out in hard copy at the Tektronix graphics terminal. The print includes the intensity values of all pixels in the horizontal scan and a printout of the image containing only pixels above or below a preselected threshold value. Experimental conditions for each image are entered on the Nova 3 terminal and can be recalled and printed.

The photograph of Figure 4 is an overall view of the experimental arrangement. The target is at lower left and the mirrors at lower right. The existing scanning mirrors were used and masked to the aperture size of the horn antenna. The data processing equipment is shown photographically in Figure 5. The terminal, Nova 3, and Colorado video appear at lower left and center and the Lexidata, joystick, printers and graphics terminal are shown at center-right.

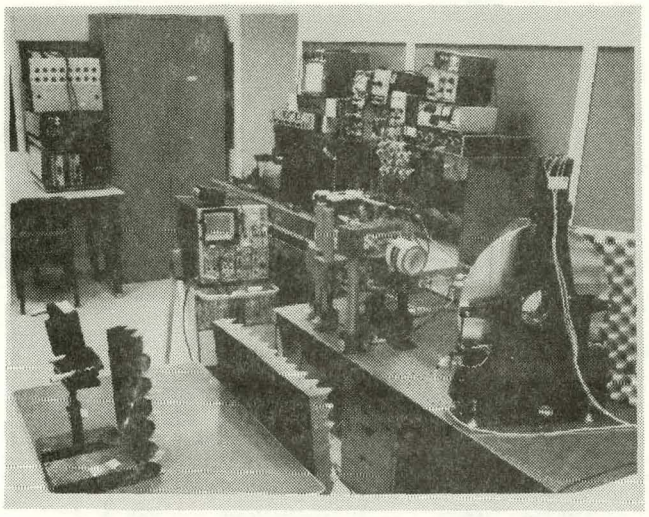

Figure 4. Overall Experimental Arrangement

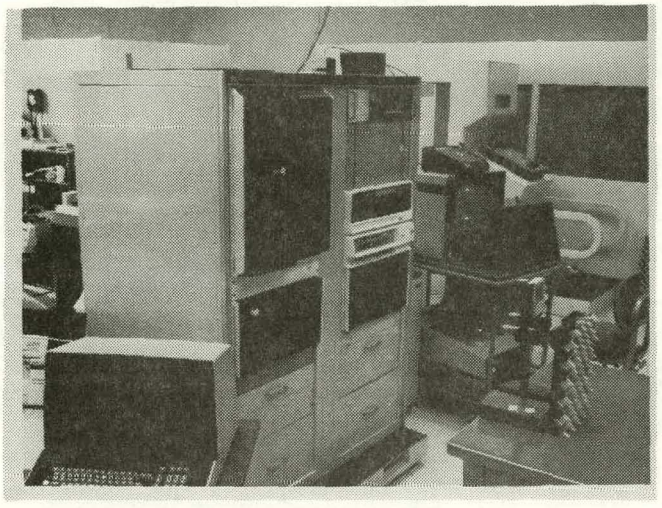

Figure 5. Data Processing and Display Equipment

All-Angle Illumination

Four methods of accomplishing all-angle illumination or the equivalent were considered as candidates for development. These are presented here and described, experimentally, in following sections.

1. The all-angle illuminating wall is an enclosure with radiating walls. The walls may consist of either a number of extended area sources, a sufficiently large number of point sources, a specular or diffuse reflecting wall illuminated by a small number of sources, or if acceptable, a cooled wall. This is a conceptually direct method, but the development of practical extended area sources or a uniformly illuminated reflecting wall, which would use only a few sources, is questionable. The intensity of fluorescent and mercury lamp sources at 3-mm wavelength has been demonstrated to be far from adequate.
2. The all-angle, retroreflecting wall is a flying-spot, auto-illuminating, scanning method proposed as a more practical alternative to the illuminating wall. This technique employs only a single source and should be a lower power, dosage, and cost method. Scanning is accomplished vertically by the flying-spot and horizontally by subject body rotation. Development of a retroreflecting wall is required. The main effort of the present work was directed toward the investigation and development of this retroreflecting/scanning search system.
3. A "lost beam" method was proposed, as a simpler version of the flying-spot retroreflecting method, in which a randomly oriented target object would appear dark against an intensely illuminated human body background. In the lost beam version, the retroreflecting surface is replaced by a highly absorbing enclosure wall. The unaligned object now reflects a colder surface in contrast to the saturated, or nearly saturated, illuminated body.
4. The direct backscatter method was the original detection concept. The body would be beam-scanned and the backscatter from target objects detected. The return detection signal level depends upon the target scattering cross section at 3 mm, target/background contrast, and the illumination intensity allowed within biological safety limits. Although calculated backscattering cross sections[10] fall off rapidly at small off-axis angles and strong contrast-limiting human body background signals exist, observations were performed during all-angle illumination experiments.

Illumination Methods

All-Angle Illuminating Wall Systems

An experimental, all-angle illumination concept is shown schematically in Figure 6. The hemispherical or geodesic inspection chamber has an internal surface which diffusely reflects millimeter waves. This surface is illuminated by two collimated 20-mW, 91-GHz,

Gunn diode oscillators, and two spherical (or aspherical) dispersing elements to illuminate the entire internal area. The diffuse reflected radiation, in turn, illuminates the human subject over approximately 2π radians. The chamber may be reduced to a more compact cylindrical shape if acceptable illumination uniformity can be achieved.

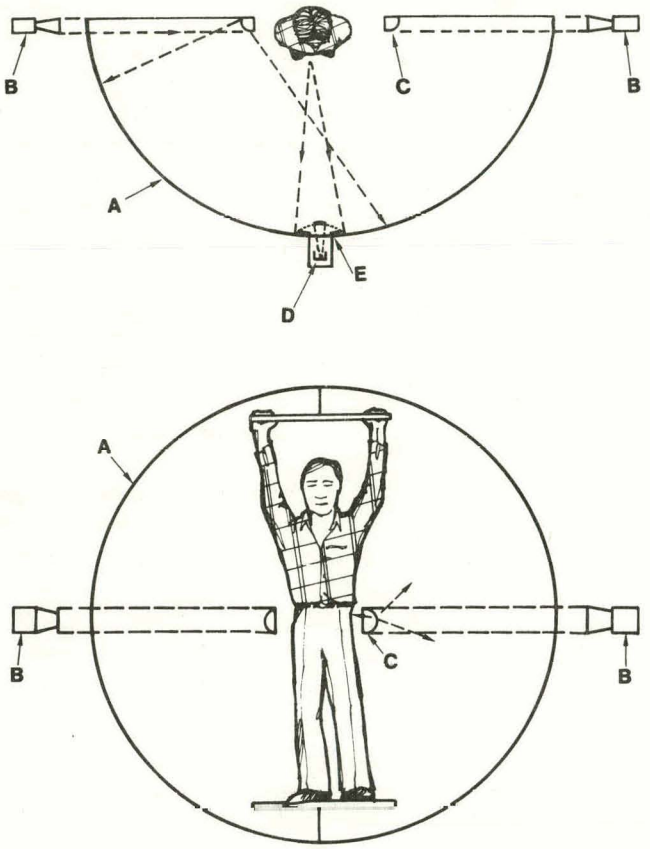

Figure 6. Diffuse Wall, All-Angle Illumination Method

The radiometer consists of a detector and an elliptical, Cassegrain optical system which may be scanned in a linear or spiral motion. This type of optical system, as used here, is advantageous because of its on-axis geometry, its compactness, and its ability to conveniently focus over a range of object distances by moving the secondary mirror. The focused Cassegrain system dimensions can also be adjusted to match the illumination intensity. In operation, the object body is step-rotated and scanned in three or four positions covering the entire body. Automatic focusing appears necessary to meet depth-of-focus requirements at extreme field-of-view diagonal distances. If a sufficiently high illumination intensity is practical, the simpler hybrid tee radiometer may be employed with small horn dimensions for acceptable resolution.

Diffuse Reflecting Wall

The source/disperser system for illuminating the reflecting wall requires further investigation before operational and cost estimates can be made. However, if the search configuration shown were successful, the cost estimate would be ~$50K. The estimated additional cost for data processing equipment consisting of scan control, Colorado video and TV monitors would be ~$12K.

LN2 Cold Wall

An LN_2 cold wall search system for metallic and composite objects can probably be developed if scenarios exist where relaxed operational criteria and cooling maintenance are acceptable. A search time of about one minute could possibly be attained and an LN_2 cold-wall system could probably be developed at moderate cost. The search system cost is estimated to be ~$50K plus the cost of data processing equipment. The cost of the scan control, Colorado video, and TV monitor is ~$12K.

Multiple-Source Wall

An illuminating wall composed of horns, power dividers, and a smaller number of sources is a direct approach which should have a high probability of success. Although the minimum number of components required for acceptable operation has not been definitely established, the number and cost is probably prohibitive. The cost of an eight-horn system using a single 20-mW source and power dividers has been quoted at $15K.

Retroreflector All-Angle Illumination System

The method shown schematically in Figure 7 was proposed as an alternative to the development of a uniform, illuminating wall. Here, the body is illuminated and scanned by a flying-spot beam system generated by a single 3-mm source. This also has the advantage of reduced irradiation of the subject, enhanced intensity/search period tradeoff, simplified scanning, no focusing requirements, and lower cost. Again, this scheme depends on the development of an enclosure wall, but the retroreflecting surface required was thought to be more attainable.

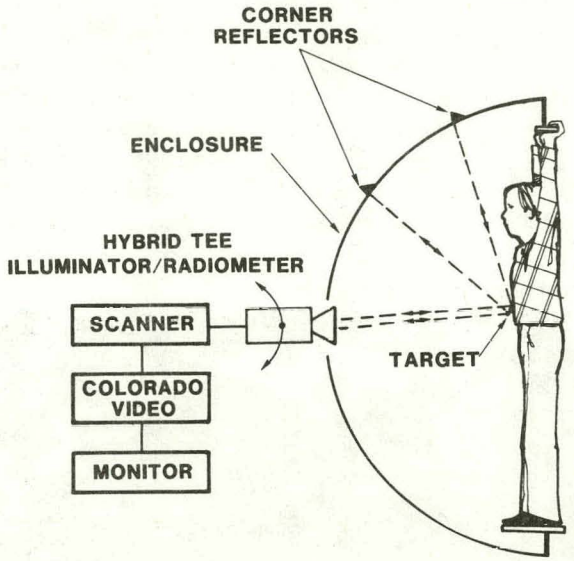

Figure 7. Retroreflector, All-Angle Illumination Method

The enclosure is a hemispherical chamber ~3 m in dia. The retroreflecting inner surface is represented by two individual corner-cube retroreflectors. The vertical-scanning hybrid tee detector/transmitter assembly shown in Figure 7 is the proposed final configuration with the horizontal scan produced by rotating the subject body. The detector signals are processed by the Colorado video unit, and the image is displayed on the TV monitor. The following data was not obtained with this arrangement, but with that shown in Figures 3 and 4 and in lieu of scanning and body rotation mechanism development.

In operation, the horn/lens assembly sweeps a collimated beam vertically across the body. The beam is reflected to the surrounding wall by the target object. The retroreflective wall surface returns the beam on approximately the same path, back to the target, and into the horn antenna and radiometer detector. The processed signal data then forms the image display on the monitor.

Retroreflective Wall Surface

Trihedral corner reflector characteristics have been reported[11] for wavelengths to about 1.5 cm. The reflector consists of three reflecting planes forming a right-angle corner. Rays entering the reflector will be triply reflected and returned along the same approximate path if they are contained within the equivalent flat plate area A_T, the entrance aperture of the corner. The area A_T is a function of the aspect angle of the radiation incident upon the reflector. The radiation outside A_T will undergo double reflection and be lost.

The corner reflector can be constructed with triangular or square sides. For a triangular trihedral at optimum orientation (radiation parallel to the symmetric axis),

$$A_T = \frac{a^2}{\sqrt{3}} \text{ and } \sigma = \frac{4\pi a^4}{3\lambda^2} \quad ,$$

where

a = length of the sides
σ = scattering cross section
λ = wavelength.

The area A outside A_T is given by

$$A = A_f - A_T = \frac{\sqrt{3}}{2} a^2 - \frac{a^2}{\sqrt{3}} = 0.29\, a^2 \quad ,$$

where A_f = the full triangle aperture area.

The power reflected P_R is

$$P_R = \frac{P_T A_R^2 A_T^2}{\lambda^4 d^4} \quad ,$$

where

P_T = power emitted
A_R = effective antenna area = $Gd^2/4\pi$, where
G = gain
d = transmitter to target distance.

All dimensions are assumed large compared to the wavelength.

The intensity of the triply reflected signal is proportional to A^2. The square corner has three times the maximum beam cross section of the triangular corner and nine times the received power. The square corner reflector returns a stronger signal, but the angular response pattern is sharper than the triangular reflector pattern. For the triangular corner the response approximates a parabaloid of revolution given by

$$\frac{A_T}{A_o} = 1 - .00076\,\delta^2, \text{ for } \delta < 26^\circ \ ,$$

where

A_T = actual cross section of the triply-reflected beam
A_o = maximum value of A along the symmetric axis
δ = deviation in degrees from the symmetric axis.

$A/A_o = 0.5$ at $\delta \approx 26^\circ$ and 0.1 at δ and W (azimuthal angle) $\approx 35^\circ$. The square corner response approximates a cone and

$$\frac{A_T}{A_o} = 1 - .0274\,\delta, \text{ for } \delta < 26^\circ \ ,$$

where

$A_T/A_o = 0.5$ at $\delta \approx 16^\circ$ and 0.1 at δ and W $\approx 35^\circ$. Sharp peaks also occur in both cases at $\delta = \pm 40^\circ$ and W $= -35^\circ$, where the alignment of two planes produces a dihedral reflection. Ray tracing estimates indicate that a corner reflector response of $\delta \approx \pm 40^\circ$ may fulfill retroreflection angular requirements for a body and realistic targets within the hemispherical enclosure.

The retroreflector dimensions are primarily a compromise between entrance aperture, target resolution, array dead area, and wavelength. As large an aperture as possible would maximize signal intensity and reduce scattering losses in this quasi-optical region of operation where the minimum desired target resolution (1 cm^2) is not large compared to the 3-mm wavelength. However, dead areas with no response will exist in a reflector array if the area between two adjacent triply reflecting areas is equal to or larger than the beam area reflected from the target. Also, a relatively large reflector will laterally displace the return beam with respect to the target diffraction effects, and angular divergence between incident and reflected beams (5 minutes nominal) will further degrade the return signal level. These factors indicate that detection of a 1-cm^2 target at 3-mm wavelength may not be possible by this method and that operation at $\delta \approx \pm 40$, with a satisfactory S/N ratio is questionable. It was estimated, however, that detection might be accomplished at about 6 cm^2 target resolution ($\sim 8\lambda$ dimensions) using corner reflectors with 25.4-mm sides.

Two available types of commercial retroreflectors were obtained to test these assumptions. These are the upper three units in Figure 8. Reflector (a) consists of 4 triangular arrays (6.9 cm on a side) composed of 60 triangular corner reflectors with 1-cm sides.* Each array is molded in plastic with vacuum-deposited, reflecting surfaces. Arrays (b) and (c) were assembled from individual square-corner reflectors constructed of vacuum-deposited glass plates.** Array (b) is composed of 14 corners, each 1.74 cm on a side (2.54-cm aperture). Array (c) is four corners, each 4.45 cm on a side (6.35-cm aperture). Array (d) is an experimental 1.9-cm dia polyethylene sphere and aluminum backing array which loosely approximates a Luneberg lens array. This was investigated as a potentially easily fabricated, inexpensive retroreflective or, with a reflective coating, diffusive surface.

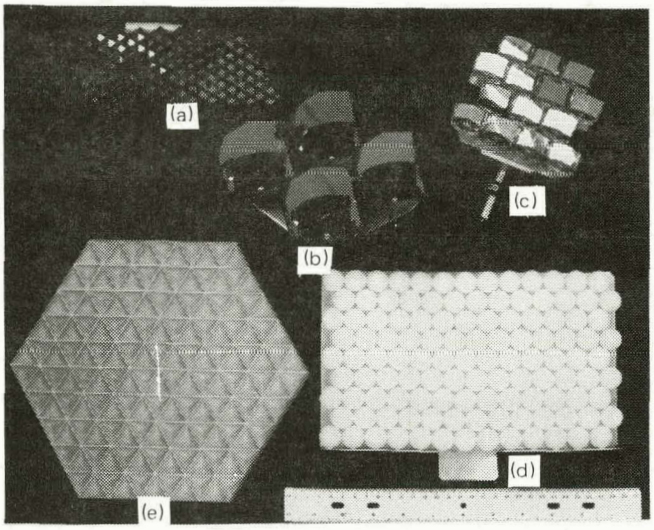

Figure 8. Retroreflector Arrays (a. 1.4-cm Triangular Array; b. 2.54-cm Square Array; c. 6.35-cm Square Array; d. 1.9-cm Diameter Polyethylene Sphere Array; e. 2.54-cm Hexagonal Array)

Figures 9 and 10 are angular response curves of the 1- and 2.54-cm corner arrays and the 1.9- and 2.54-cm-dia polyethylene sphere arrays. These early interferometric mode observations employed the 7.6-cm-dia horn/lens antenna, hybrid tee, 91.0-GHz Gunn diode modulated at 1 kHz, and lock-in amplifier. The 7.6-cm horn/lens antenna radiation pattern is shown in Figure 11. The beam was nonscanning, but was reflected by a 7.6-cm-square aluminum plate to the reflectors to simulate the final application. Signal intensities at each incidence angle are peak-to-peak values obtained by translating the reflector plate to vary the beam path length by $\lambda/4$. The 2.54-cm

*SAI Technology Company, 4060 Sorrento Valley Blvd, San Diego, CA 92121

**Precision Lapping and Optical Co., Inc, PO Box 68, 43 Railroad Ave., Valley Stream, NY 11582

square-corner array curve exhibits the characteristic envelope shape and contains cyclic variations attributed to diffraction,[10] individual corner distance variations with array rotation about a central axis, and beam aperture averaging. The 1-cm triangular-corner results are lower in intensity, obtain over only ~25°, and do not display the characteristic shape at this orientation and wavelength. The sphere curves differ in shape and are prohibitively lower in intensity by ~25 dB.

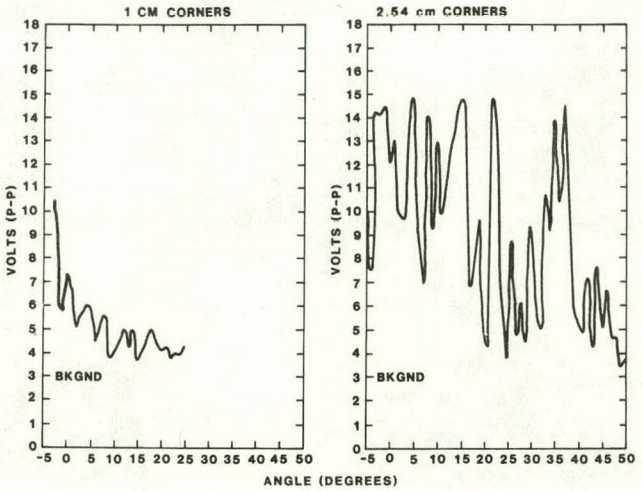

Figure 9. Angular Response of 1-cm Triangular and 2.54-cm Square Retroreflector Arrays

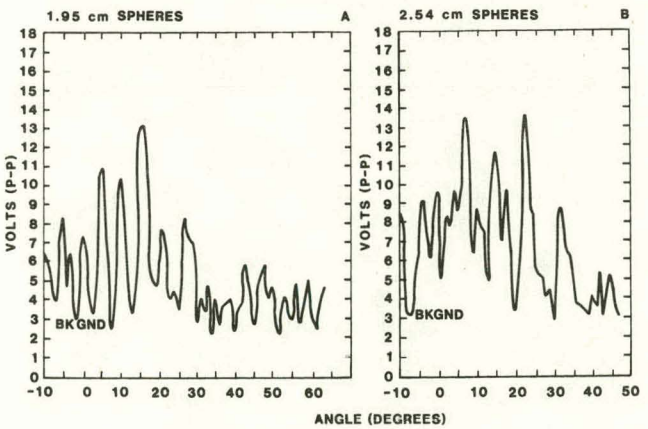

Figure 10. Angular Response of 1.9-cm and 2.54-cm Diameter Polyethylene Spheres

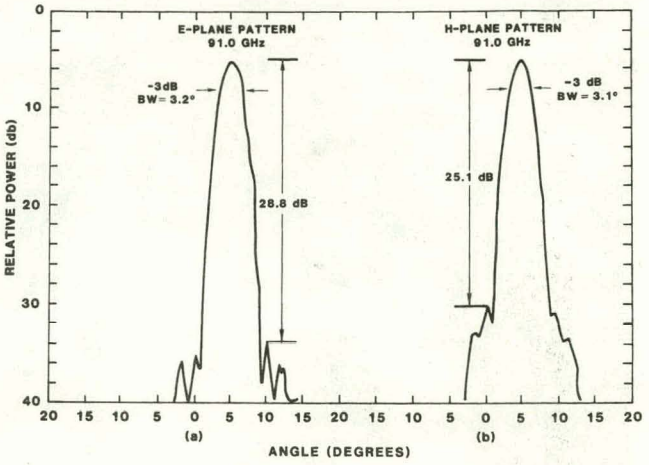

Figure 11. 7.6-cm-Diameter Horn/Lens Antenna Radiation Patterns

Experimental Results

Experimental Apparatus

Observations were made with the experimental arrangement in Figures 2 through 5. The retroreflector array positioned directly above the horn/lens antenna (Figure 4) represents a section of enclosure wall. Flat plate aluminum targets were 3.2-, 5.1- and 7.6-cm square. Both 7.6- and 2.54-cm-dia horn/lens antennas were employed. The 2.54-cm antenna appears in Figure 12(a) and is described in Appendix B. The target plates were 145 cm from the first mirror and 252 cm from the horn antenna. Samples were oriented for optimum signal levels, unless otherwise noted, in lieu of a complete reflecting wall. Values given in decibles denote attenuation of illumination beam power.

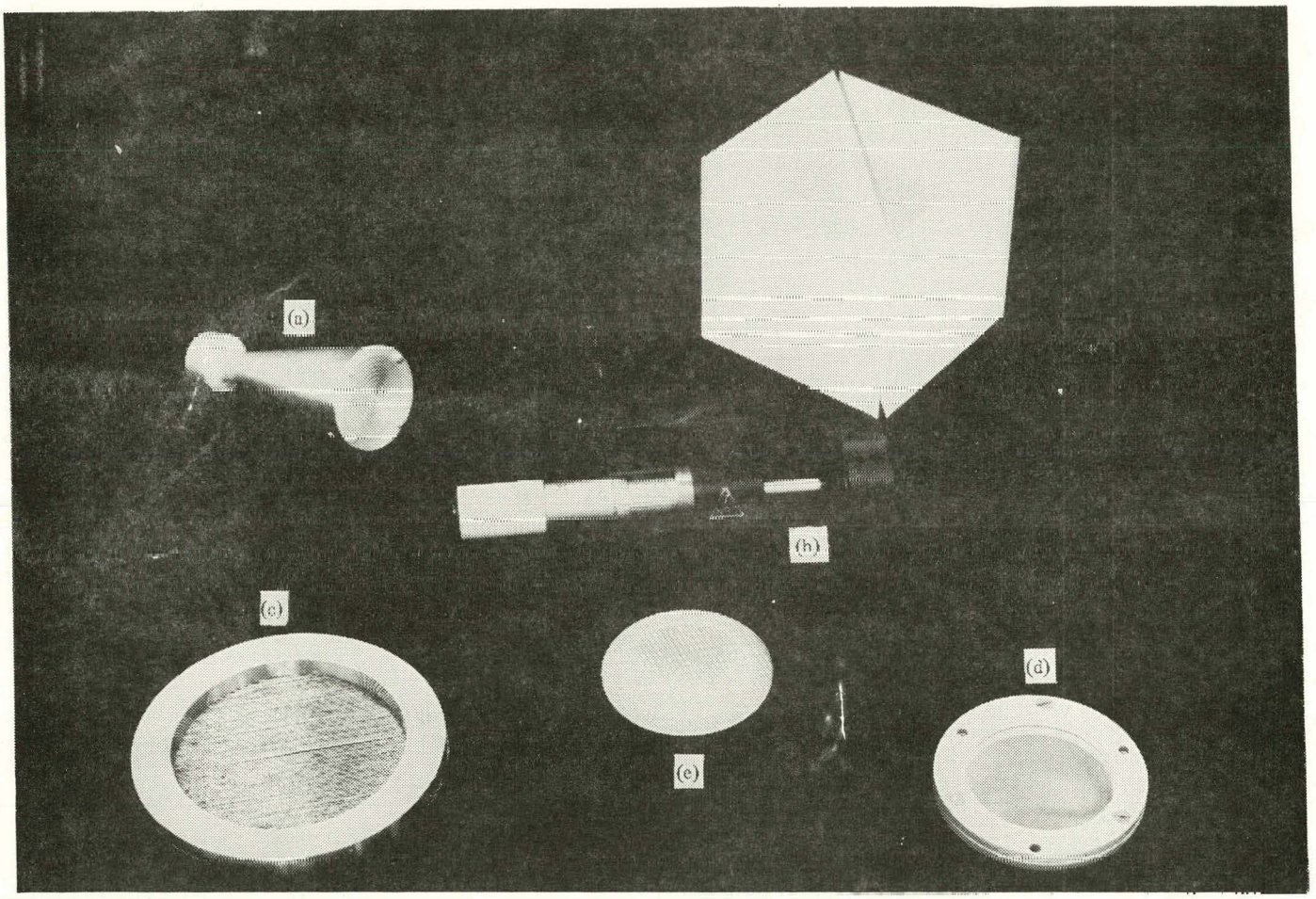

Figure 12. Near-Millimeter-Wave Quasi-Optical Components (a. 2.54-cm Horn/Lens Antenna; b. Double Dielectric Prism Beam Splitter; c. 6-cm Diameter Wire Grid Polarizer; d. 3.81-cm Wire Grid Polarizer; e. 3.8-cm Rexolite Lens)

Interferometric Results

Observations began in the full interferometric mode. The displayed image field of view was zoomed by a factor of 4 and is about 20 cm long x 10 cm high at the target plane. The assymetry is caused by a factor of 2 difference in mirror scans and 10% nonlinearity in the CRT display. Figures 13 and 14 are photographic and printed results displaying typical interferometric effects. The bright and dark interference patterns on the left and right sides of the image are caused by radiation backscattered primarily from the mirror system. Masking reduced this to the present level with the 7.6-cm-dia antenna beam. The 2.54-cm-dia antenna produces objectionably enhanced interference effects in the image, compared to the 7.6-cm-dia antenna; this difference is attributed to reduced aperture averaging.

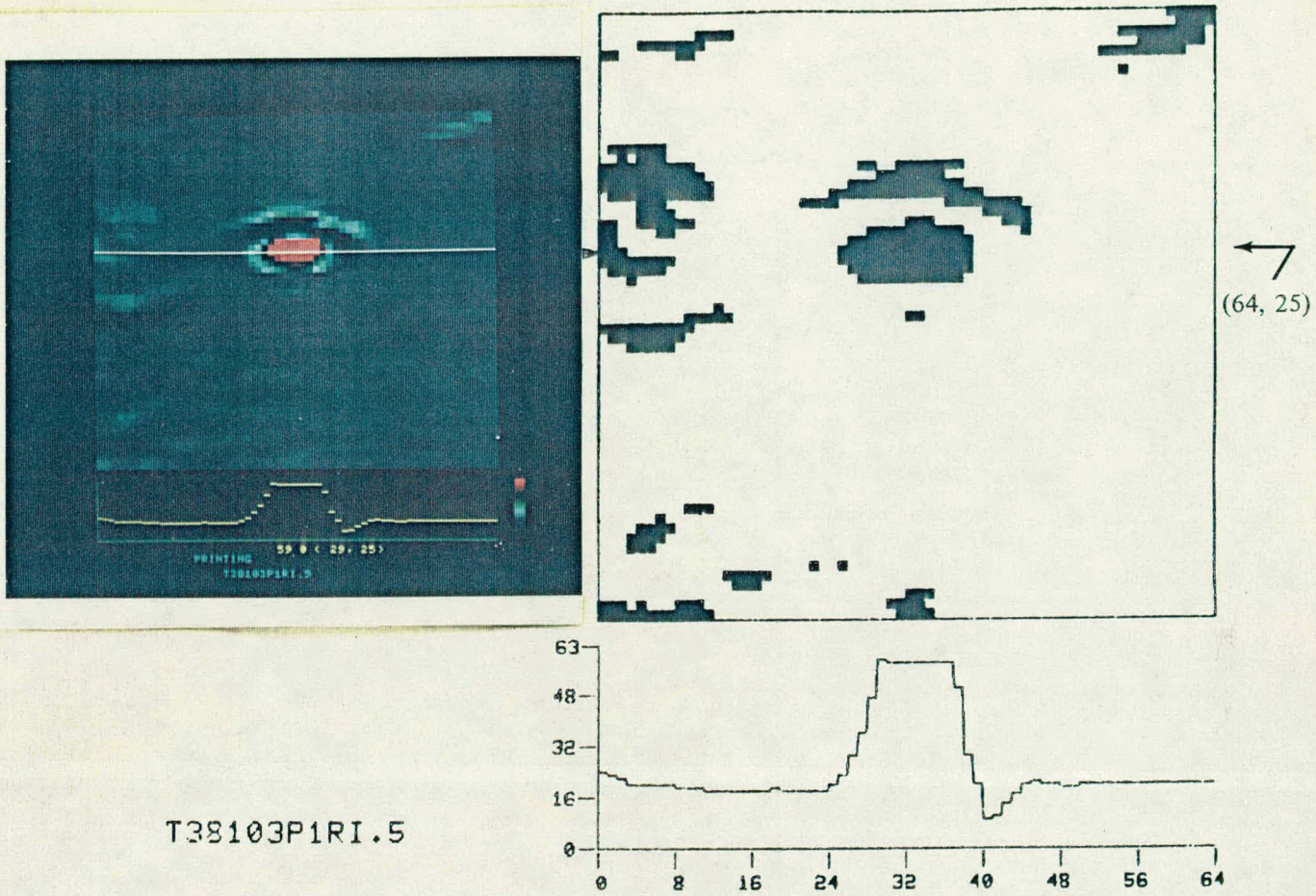

THE DATA VALUES IN THE HORIZONTAL SLICE BEGINNING AT (0, 25) ARE:

```
24 23 22 20 20 20 20 20 19 19 19 18 18 18 18 18
18 18 19 18 18 18 18 18 20 23 29 36 47 59 58 58
58 58 58 58 58 50 29 20  9 10 14 17 20 21 20 20
19 19 20 20 20 20 20 20 20 20 20 20 20 20 20 20
```

(a) Full Interferometric, 39-dB Attenuation, S/N = 2.7:1

```
PLOT IMAGE ? (1=YES,0=NO) 1
ENTER MINIMUM GRAY SCALE TO BE PLOTTED 22
```

Figure 13. Interferometric Results, Eccosorb Background; 7.6-cm-Diameter Horn/Lens Antenna, 7.6-cm Target Plate, and 2.54-cm Retroreflector Array

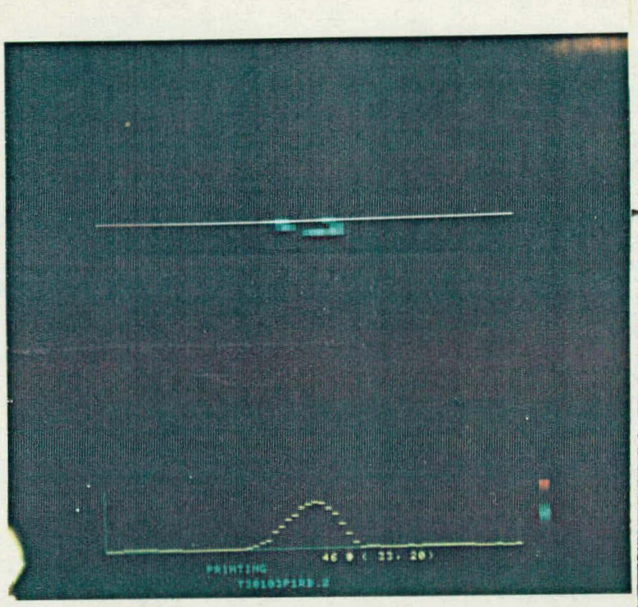

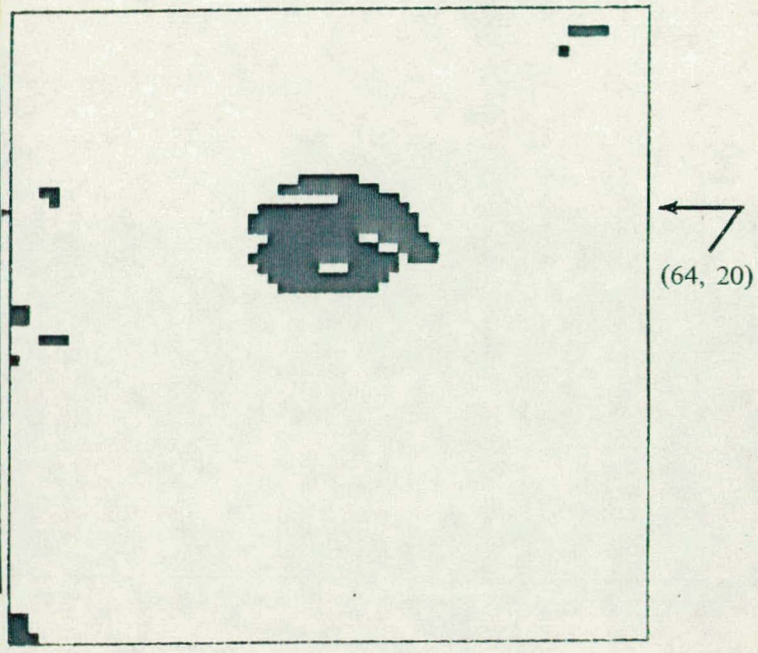

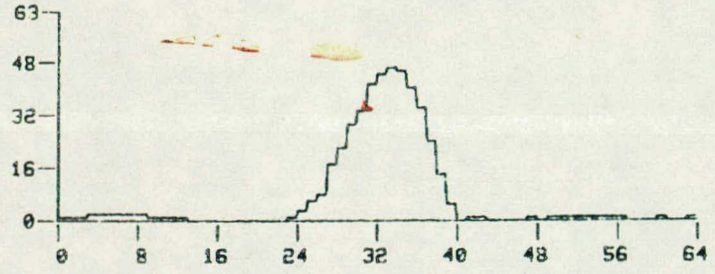

T38103P1RB.2

THE DATA VALUES IN THE HORIZONTAL SLICE BEGINNING AT (0, 20) ARE:

1	1	1	2	2	2	2	2	2	1	1	1	1	0	0	0
0	0	0	0	0	0	0	1	3	6	8	17	22	29	33	41
44	46	45	40	34	24	14	5	0	1	1	0	0	0	0	1
0	1	1	1	1	1	1	1	1	0	0	0	1	0	0	1

(b) 41-dB Attenuation, S/N = 11.5:1

PLOT IMAGE ? (1=YES,0=NO) 1
ENTER MINIMUM GRAY SCALE TO BE PLOTTED 4

Figure 13. (Continued)

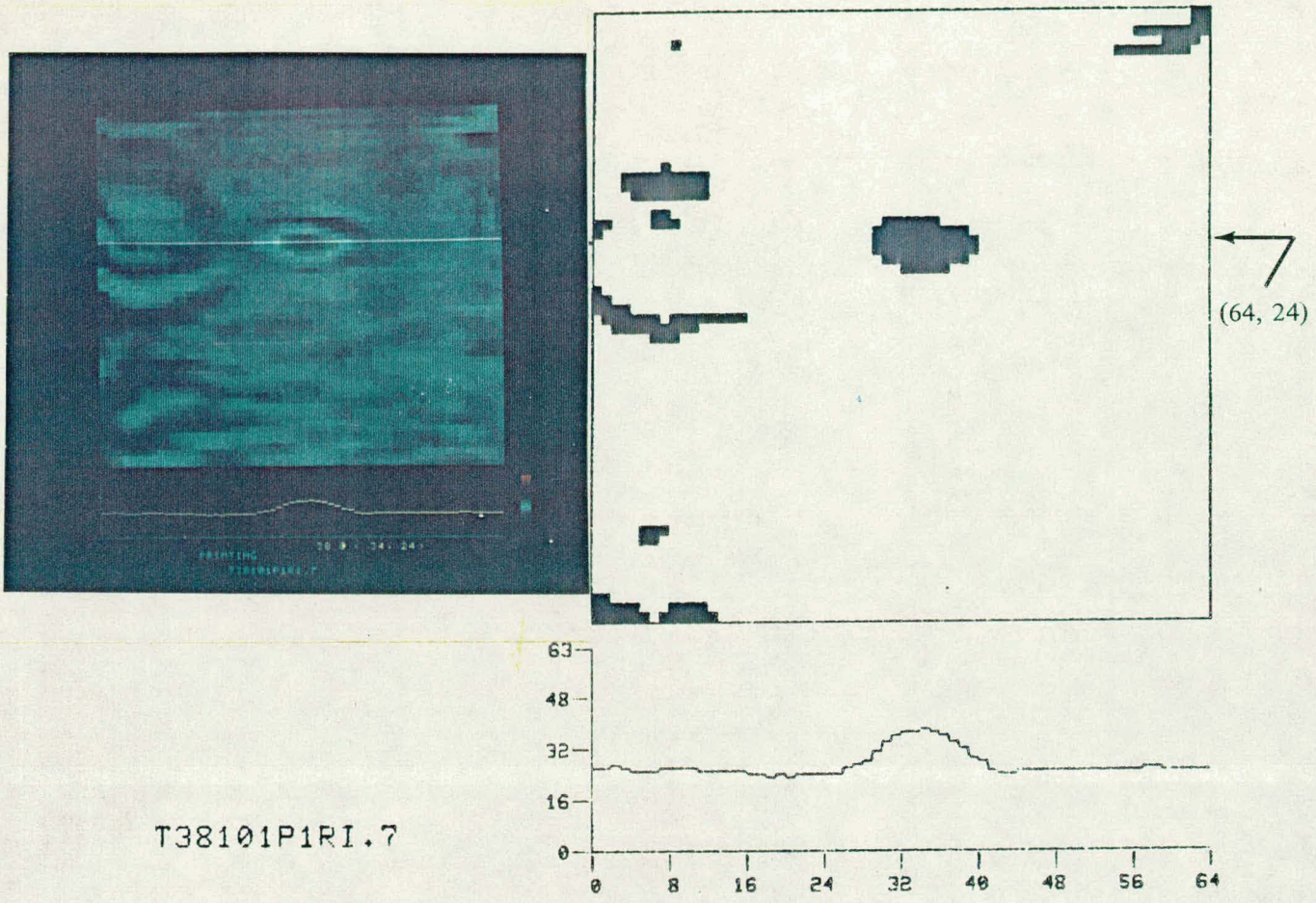

THE DATA VALUES IN THE HORIZONTAL SLICE BEGINNING AT (0, 24) ARE:

```
26 26 27 26 25 25 25 26 26 26 26 25 25 25 25 25
24 24 23 24 23 24 24 24 24 24 26 27 28 31 34 36
37 37 38 37 36 34 32 29 28 25 24 24 25 25 25 25
25 25 25 25 25 25 25 25 25 26 26 25 25 25 25 25
```

(a) Full Interferometric, 29-dB Attenuation, S/N = 1.3:1

```
PLOT IMAGE ? (1=YES,0=NO) 1
ENTER MINIMUM GRAY SCALE TO BE PLOTTED 29
```

Figure 14. Interferometric Results, Eccosorb Background; 7.6-cm-Diameter Horn/Lens Antenna, 3.2-cm Target Plate, and 2.54-cm Retroreflector Array

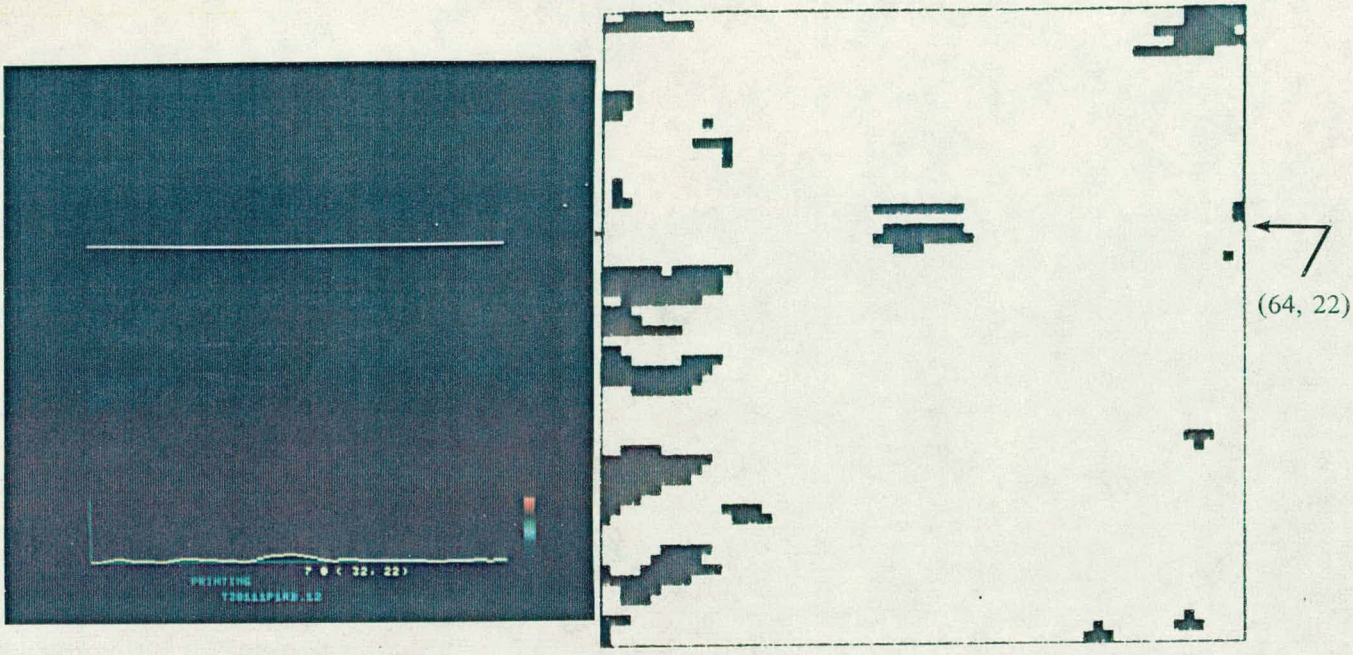

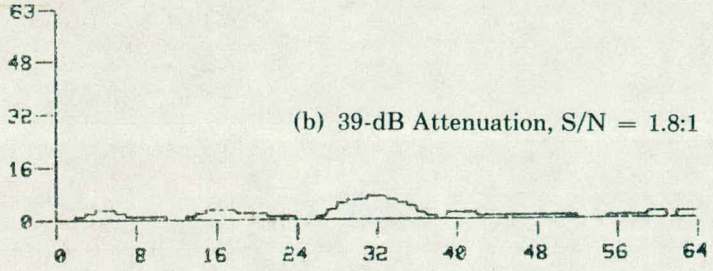

(b) 39-dB Attenuation, S/N = 1.8:1

T32111P1RB.12

THE DATA VALUES IN THE HORIZONTAL SLICE BEGINNING AT (0, 22) ARE:

0	0	1	2	3	3	2	1	1	1	1	0	0	1	2	3
3	3	2	2	2	1	1	1	0	0	1	3	5	6	6	7
7	6	5	4	2	1	0	2	2	2	1	1	1	1	1	1
1	1	1	1	0	0	0	1	1	1	1	2	2	0	2	2

PLOT IMAGE ? (1=YES,0=NO) 1
ENTER MINIMUM GRAY SCALE TO BE PLOTTED 4

Figure 14. (Continued)

S/N ratios were 2.7 and 1.3 for the 7.6- and 3.2-cm plates, respectively. S/N ratios in this report are minimums derived from target peak signal levels and maximum background pixel levels, and ignore the bright interference fringes at the sides. Observations confirm system operation, but the effects of aperture averaging and distance variation during scanning do not sufficiently reduce the signal distance-dependency to provide an acceptable method.

Radiometric Results

Figure 15 shows results with the 2.54-cm horn/lens antenna and 7.6- and 3.2-cm target plates reflecting directly back into the detector. (No retroreflectors were used.) The hybrid tee detector was nulled on the Eccosorb background. Comparable return signals required an increase of 10 dB in beam intensity for the 3.2-cm target, which enhances the backscattering and residual interference effects. A great reduction in S/N ratio, 54 to 2.4, is evident for the 3.2-cm plate.

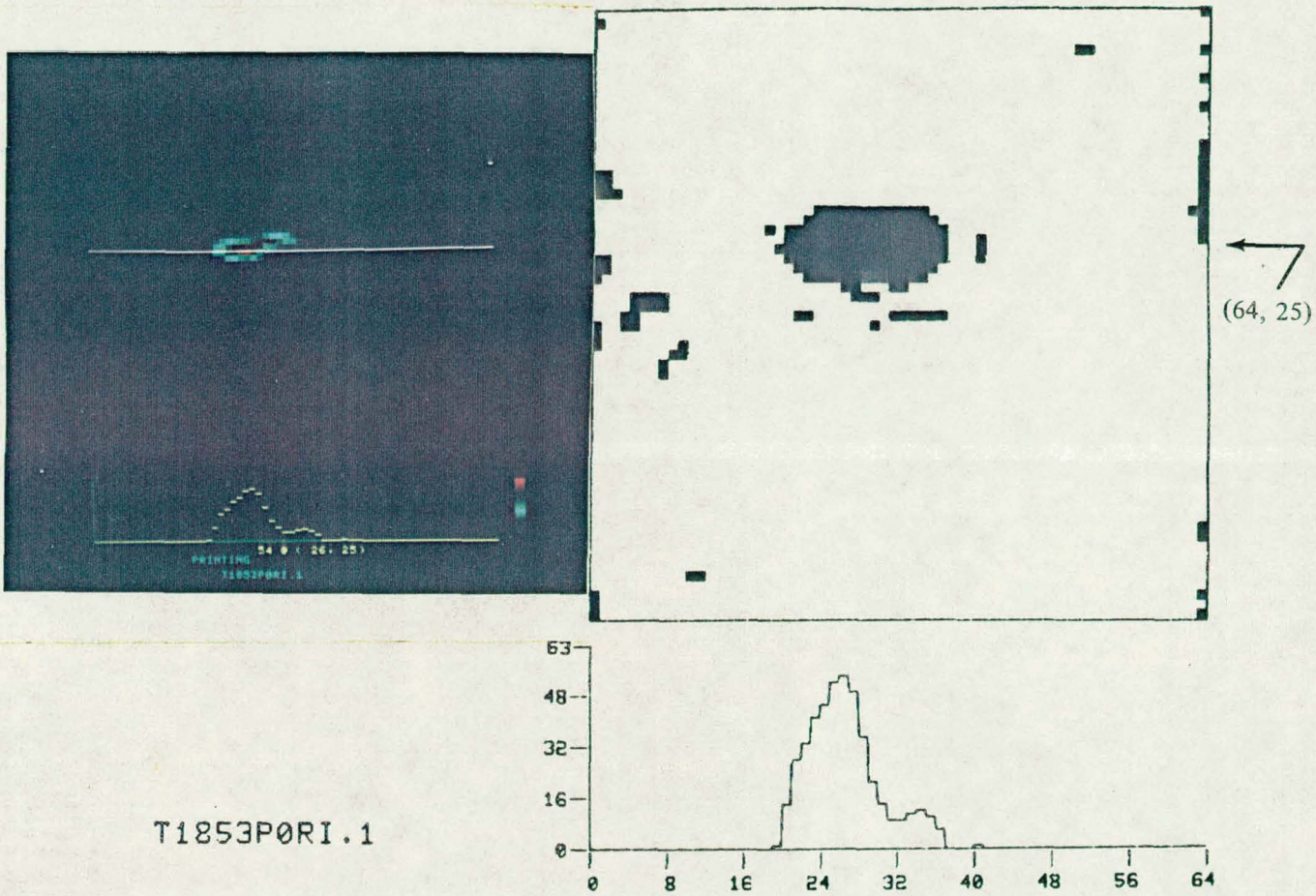

THE DATA VALUES IN THE HORIZONTAL SLICE BEGINNING AT (0, 25) ARE:

0	0	0	0	0	0	0	0	0	0	0	0	0	0	0	0
0	0	0	1	14	28	33	41	45	52	54	49	35	21	14	9
9	11	12	10	6	0	0	0	1	0	0	0	0	0	0	0
0	0	0	0	0	0	0	0	0	0	0	0	0	0	0	0

(a) 7.6-cm Target Plate, 30-dB Attenuation, S/N ≥54:1

PLOT IMAGE ? (1=YES,0=NO) 1
ENTER MINIMUM GRAY SCALE TO BE PLOTTED 1

Figure 15. Radiometric Results; 2.54-cm-Diameter Horn/Lens Antenna, Direct Return Reflection From Target Plate

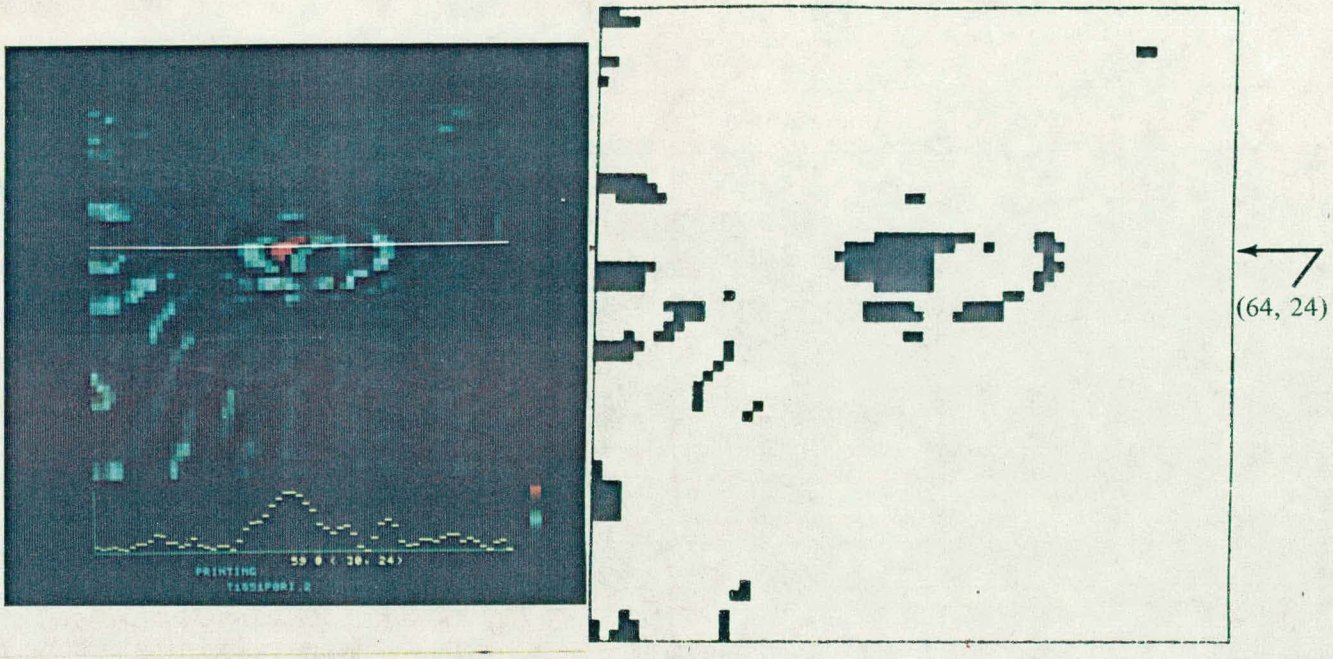

THE DATA VALUES IN THE HORIZONTAL SLICE BEGINNING AT (0, 24) ARE:

6	4	5	6	4	3	6	9	9	12	18	17	10	10	6	8
14	7	5	3	6	6	2	11	23	29	30	36	46	53	59	59
56	48	41	27	23	18	23	25	17	4	0	13	27	31	25	9
5	6	11	11	9	13	16	16	9	12	9	4	1	8	10	1

(b) 3.2-cm Target Plate, 20-dB Attenuation, S/N = 2.4:1

PLOT IMAGE ? (1=YES,0=NO) 1
ENTER MINIMUM GRAY SCALE TO BE PLOTTED 25

Figure 15. (Continued)

Significant results were not obtained with the 2.54-cm-dia antenna and the 3.2-cm plate and both the 1- and 2.54-cm retroreflector arrays. Data for the 7.6-cm target plate with these retroreflectors and human body background appear in Figure 16. Interference effects are again visible at these beam intensities.

The data printed in (b) was processed at a lower threshold level making the body background signals visible above the target area. The background below the target area is Eccosorb. The body background signals can be eliminated with a resultant S/N ratio of ~6:1, twice that of the 1-cm array.

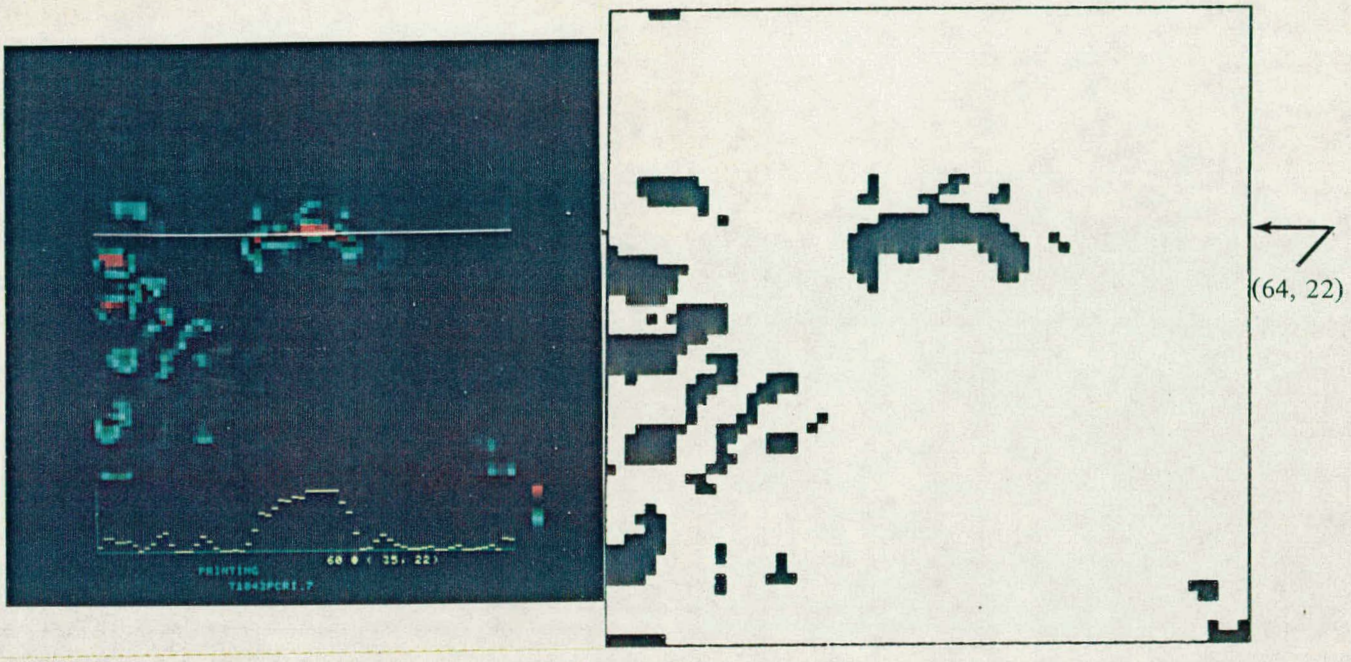

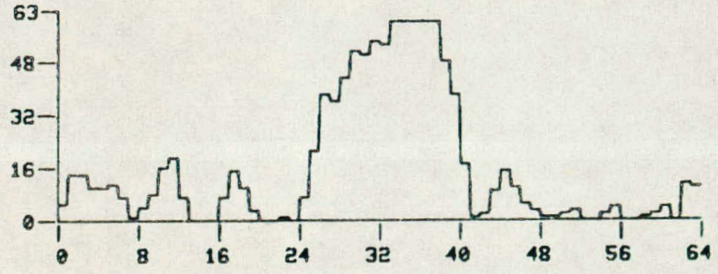

T1843PCRI.7

THE DATA VALUES IN THE HORIZONTAL SLICE BEGINNING AT (0, 22) ARE:

```
  5 14 14 10 10 11  7  1  4  8 16 19  7  0  0  0
  7 15 10  3  0  0  1  0  7 21 38 36 43 51 50 54
 53 60 60 60 60 60 48 38 17  1  2  9 15 10  5  3
  1  1  2  3  0  0  2  4  0  0  1  2  4  0 11 10
```

(a) 7.6-cm Target Plate, 1-cm Retroreflector Array, Eccosorb Background, 19-dB Attenuation, S/N = 3:1

PLOT IMAGE ? (1=YES,0=NO) 1
ENTER MINIMUM GRAY SCALE TO BE PLOTTED 20

Figure 16. Radiometric Results; 1-cm and 2.54-cm Retroreflector Array, Eccosorb and Human Body Background

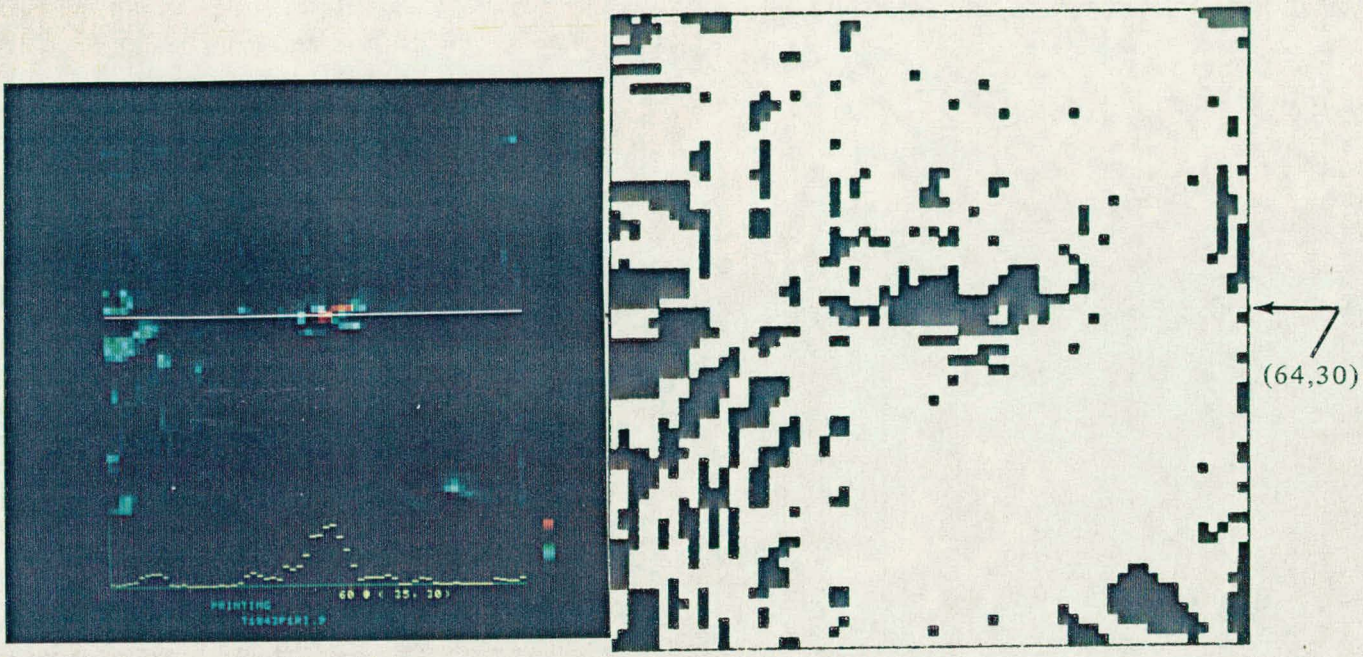

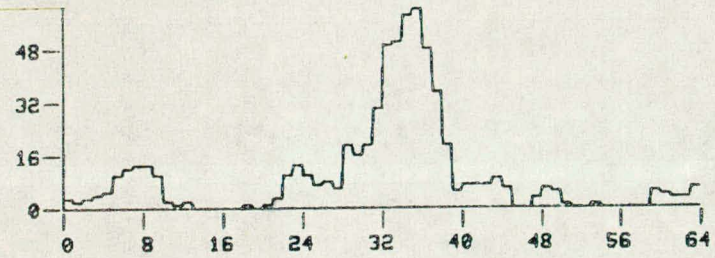

T1843P1RI.9

THE DATA VALUES IN THE HORIZONTAL SLICE BEGINNING AT (0, 30) ARE:

3	2	3	4	5	10	12	13	13	10	2	1	2	0	0	0
0	0	1	0	1	3	10	13	10	7	8	6	19	16	19	30
49	50	58	60	48	35	19	5	7	7	7	9	6	0	0	3
6	5	1	0	0	1	0	0	0	0	0	5	4	3	3	6

PLOT IMAGE ? (1=YES,0=NO) 1
ENTER MINIMUM GRAY SCALE TO BE PLOTTED 7

(a) 7.6-cm Target Plate, 1-cm Retroreflector Array, Eccosorb Background, 19-dB Attenuation, S/N = 3:1

Figure 16. (Continued)

Figures 17, 18, and 19 are a series of data for the 7.6-cm-dia antenna; they compare 3.2-, 5.1- and 7.6-cm plates in combination with 1-, 2.54- and 6.35-cm retroreflector arrays. Results are compiled in Table 1. In each case, signal levels were adjusted, as nearly as possible, to 63 gray levels making attenuation values a measure of relative intensities. It is apparent that the 2.54-cm-dia antenna is useful only with large targets. The 7.6-cm-dia antenna gives good results, especially with the 6.35-cm array.

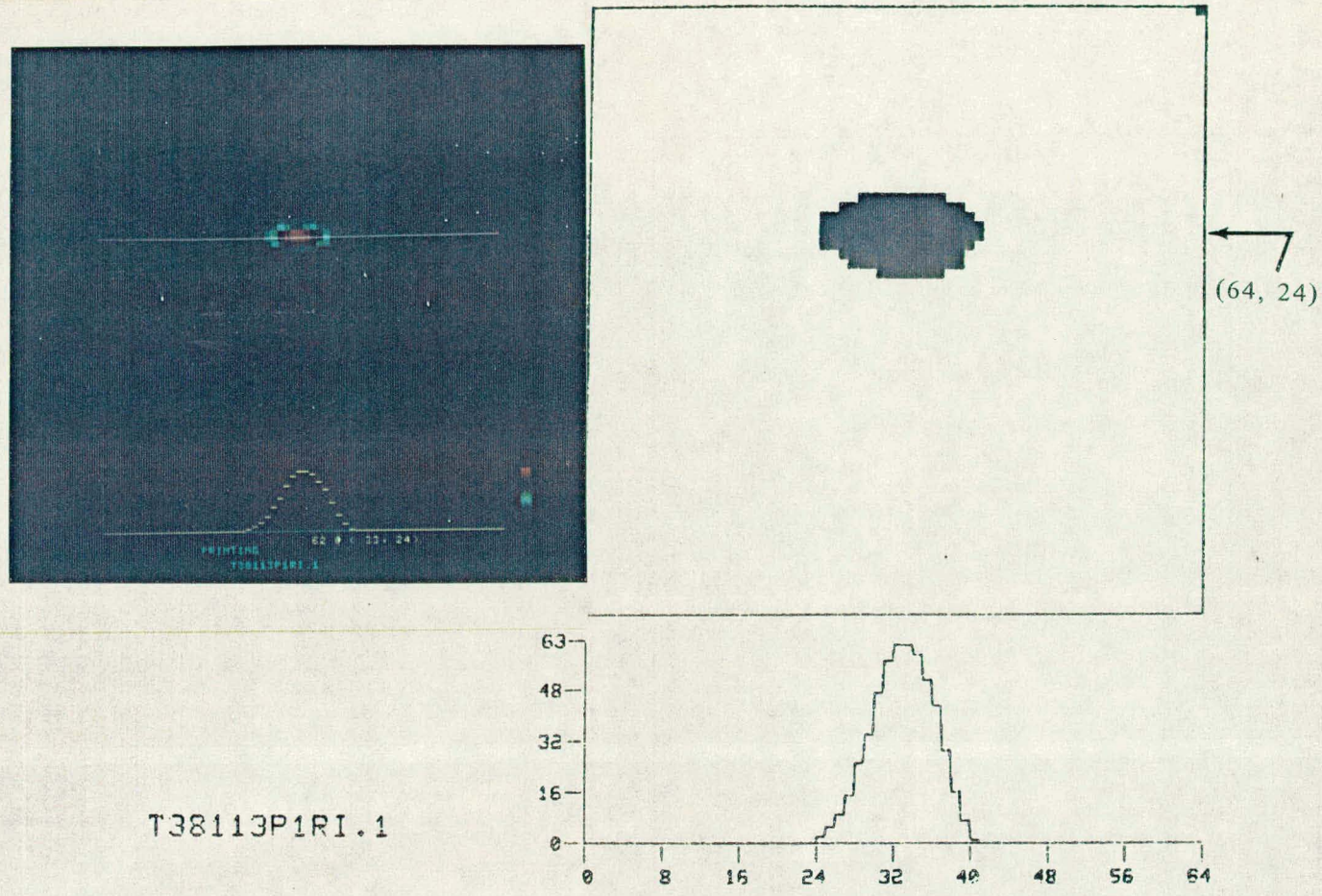

THE DATA VALUES IN THE HORIZONTAL SLICE BEGINNING AT (0, 24) ARE:

0	0	0	0	0	0	0	0	0	0	0	0	0	0	0	0
0	0	0	0	0	0	0	0	2	5	9	15	25	34	47	57
62	62	59	51	43	29	16	7	1	0	0	0	0	0	0	0
0	0	0	0	0	0	0	0	0	0	0	0	0	0	0	0

(a) 7.6-cm Target Plate, 2.5-cm Retroreflector Array, 39-dB Attenuation, S/N ≥62:1

PLOT IMAGE ? (1=YES,0=NO) 1
ENTER MINIMUM GRAY SCALE TO BE PLOTTED 1

Figure 17. Radiometric Results; 7.6-cm-Diameter Horn/Lens Antenna, 7.6-cm Target Plate, Eccosorb Background

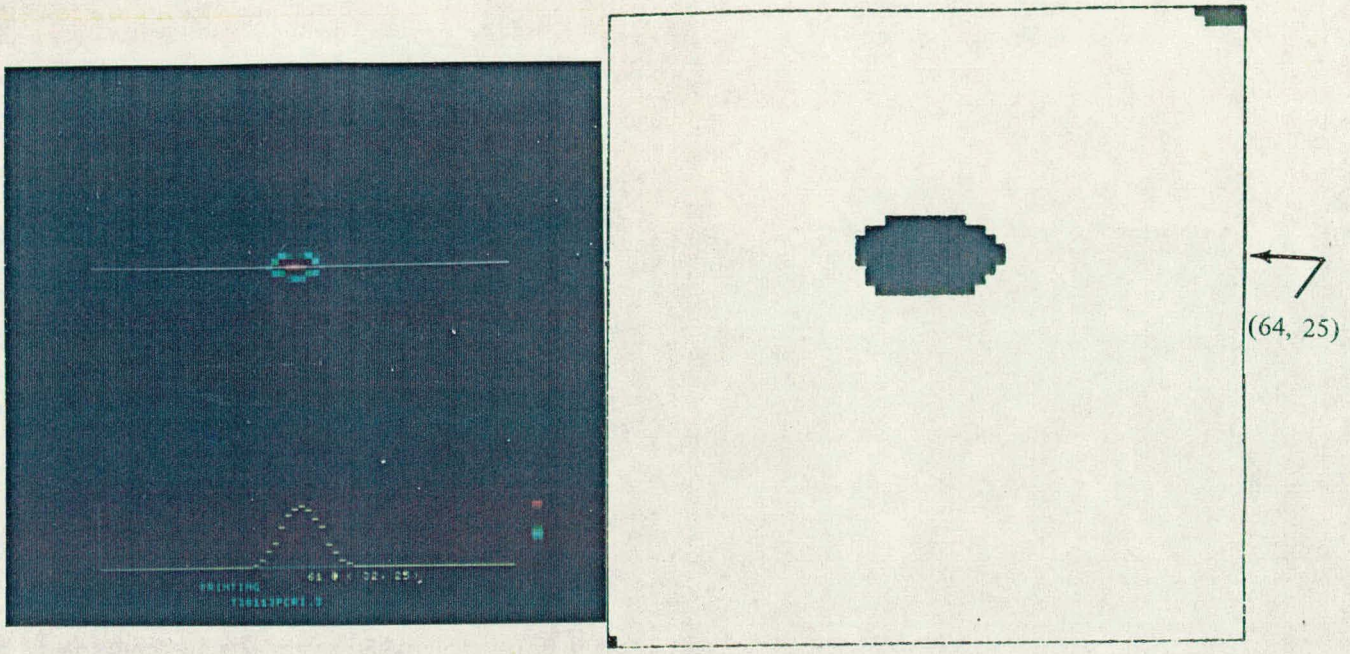

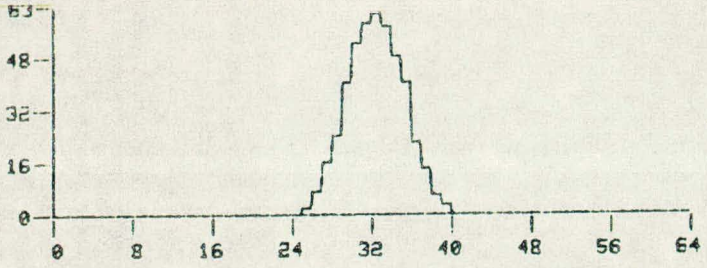

T38113P0RI.3

THE DATA VALUES IN THE HORIZONTAL SLICE BEGINNING AT (0, 25) ARE:

0	0	0	0	0	0	0	0	0	0	0	0	0	0	0	0
0	0	0	0	0	0	0	0	0	2	7	16	24	40	52	58
61	57	48	40	22	14	6	3	0	0	0	0	0	0	0	0
0	0	0	0	0	0	0	0	0	0	0	0	0	0	0	0

(b) 7.6-cm Target Plate, 1-cm Retroreflector Array, 35-dB Attenuation, S/N ≥61:1

PLOT IMAGE ? (1=YES,0=NO) 1
ENTER MINIMUM GRAY SCALE TO BE PLOTTED 1

Figure 17. (Continued)

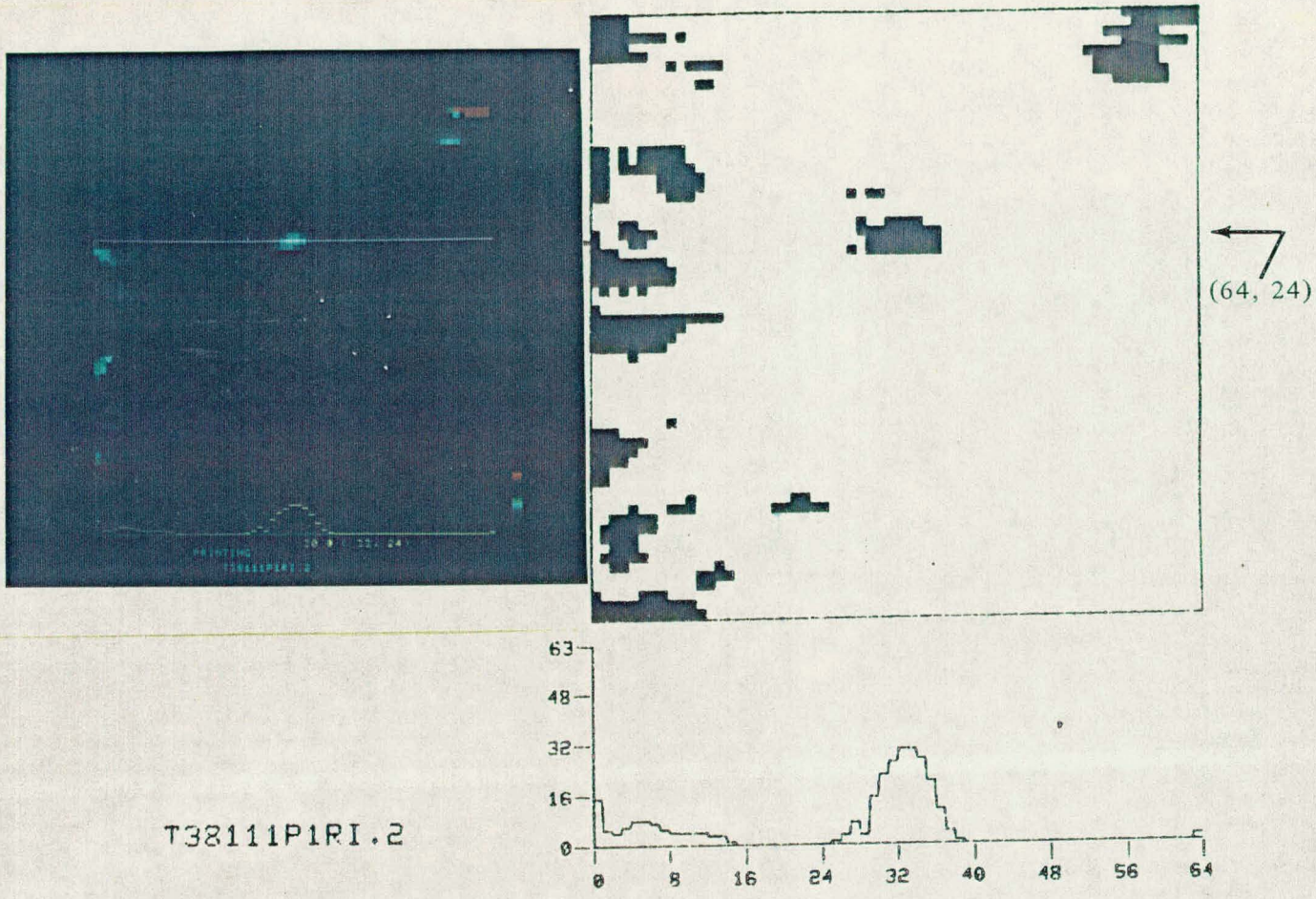

THE DATA VALUES IN THE HORIZONTAL SLICE BEGINNING AT (0, 24) ARE:

15	5	4	6	8	8	7	5	4	4	4	4	3	2	1	0
0	0	0	0	0	0	0	0	0	1	3	7	3	15	22	26
30	30	27	20	11	4	1	0	0	0	0	0	0	0	0	0
0	0	0	0	0	0	0	0	0	0	0	0	0	0	0	2

(a) 3.2-cm Target Plate, 2.54-cm Retroreflector Array, 22-dB Attenuation, S/N = 3.8:1

PLOT IMAGE ? (1=YES,0=NO) 1
ENTER MINIMUM GRAY SCALE TO BE PLOTTED 8

Figure 18. Radiometric Results; 7.6-cm-Diameter Horn/Lens Antenna, 3.2-cm Target Plate, Eccosorb Background

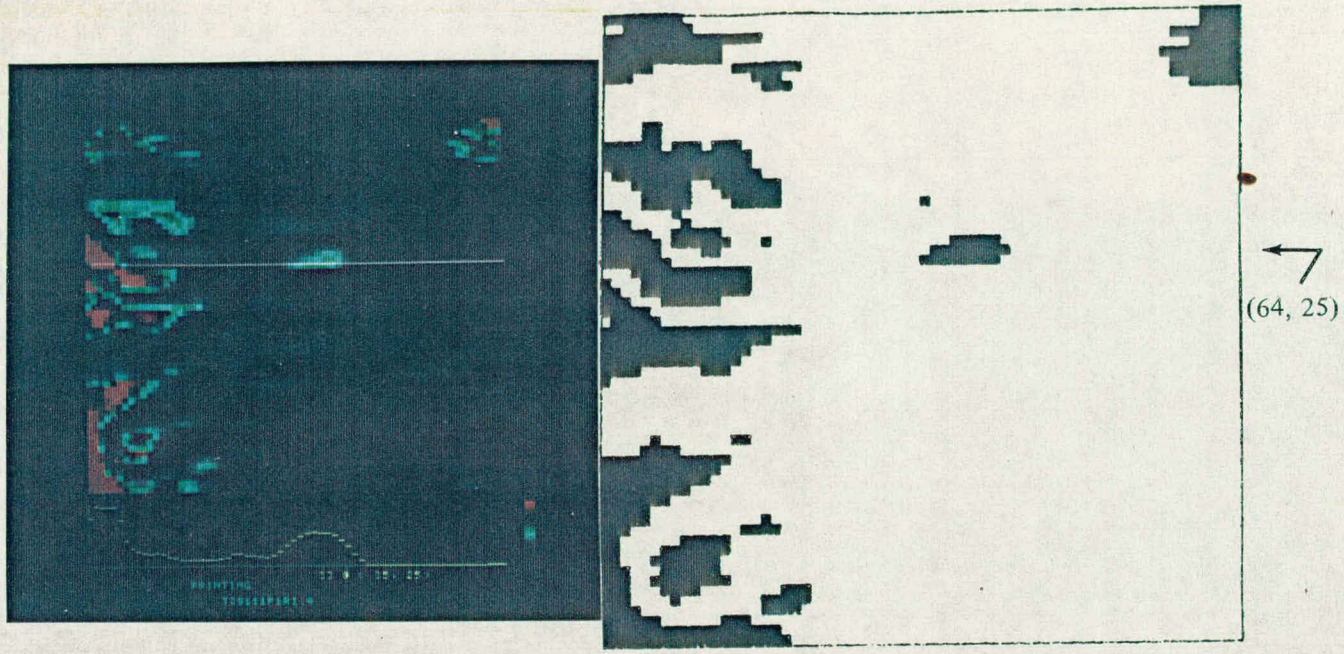

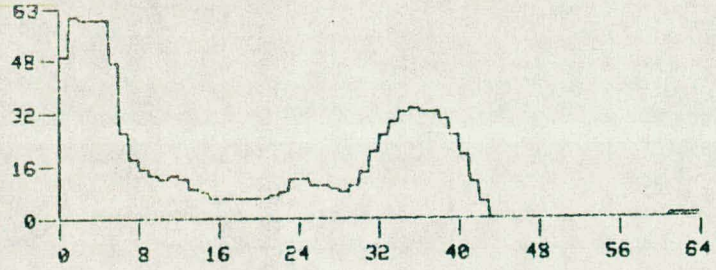

T38111PERI.4

```
THE DATA VALUES IN THE HORIZONTAL SLICE BEGINNING AT (  0, 25) ARE:

 49 61 60 60 60 47 26 18 15 13 12 13 12  9  8  6
  6  6  6  6  6  7  8 12 12 10 10  9  8 10 14 20
 25 29 32 33 32 32 30 25 19 11  5  0  0  0  0  0
  0  0  0  0  0  0  0  0  0  0  0  0  0  1  1  1

PLOT IMAGE ? (1=YES,0=NO) 1
ENTER MINIMUM GRAY SCALE TO BE PLOTTED 21
```

(b) 3.2-cm Target Plate, 1-cm Retroreflector Array, 18-dB Attenuation, S/N = 1.6:1

Figure 18. (Continued)

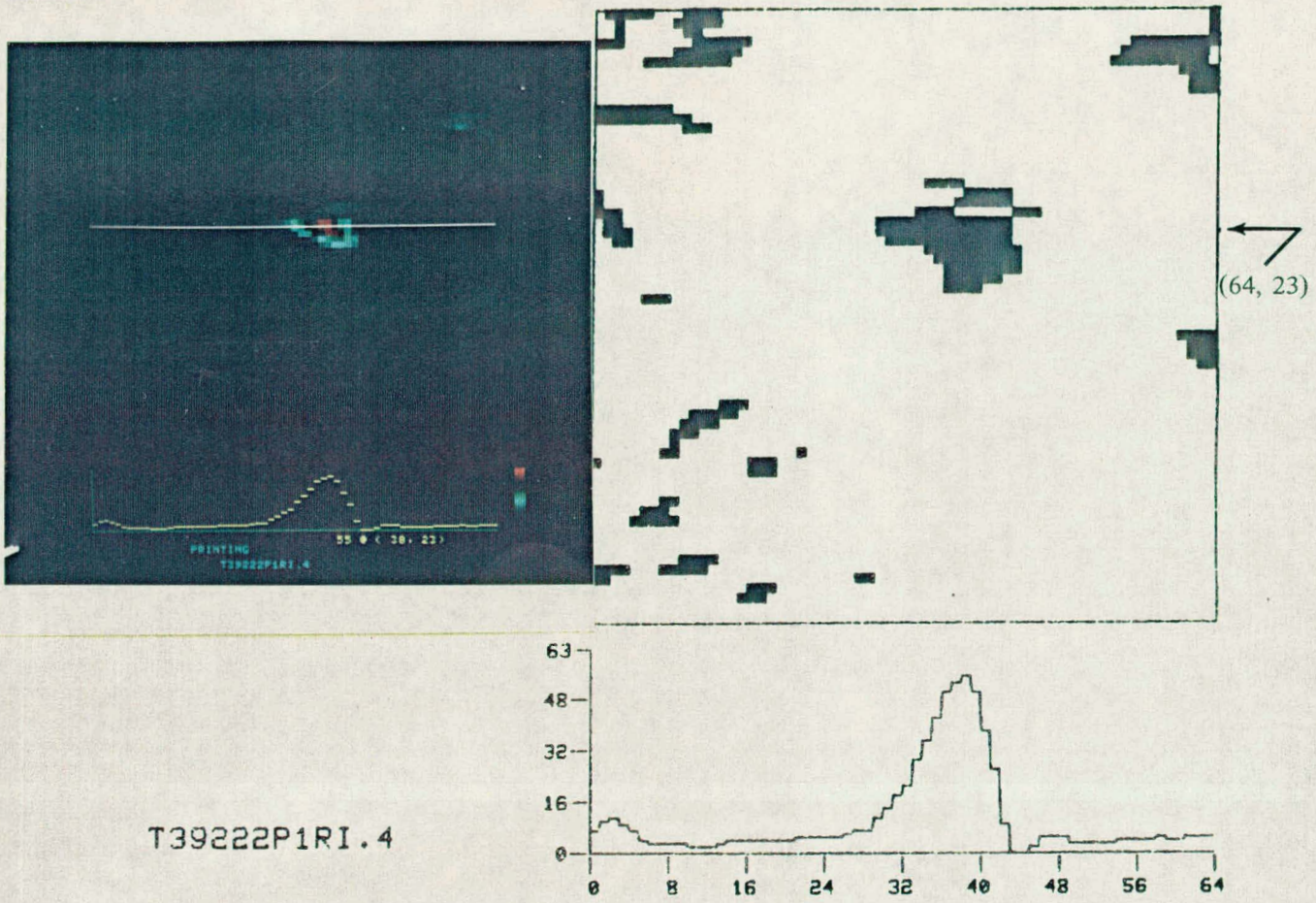

THE DATA VALUES IN THE HORIZONTAL SLICE BEGINNING AT (0, 23) ARE:

7	10	11	9	7	4	3	3	3	3	2	2	2	3	4	4
4	4	4	4	4	5	5	5	5	5	6	7	7	11	14	18
21	29	35	42	50	53	55	50	38	26	9	0	0	2	5	5
5	3	3	3	3	3	4	4	4	4	5	4	4	5	5	5

5.1-cm Target Plate, 2.54-cm Retroreflector Array, 30-dB Attenuation, S/N = 9:1

PLOT IMAGE ? (1=YES,0=NO) 1
ENTER MINIMUM GRAY SCALE TO BE PLOTTED 6

Figure 19. Radiometric Results, 7.6-cm-Diameter Horn/Lens Antenna, 5.1-cm Target Plate, Eccosorb Background

Table 1. Radiometric Results

Target Plate (cm)	Retroreflector Array (cm)	S/N Ratio	Attenuation (dB)
2.54-cm-dia Horn Lens Antenna			
7.6	1.00	3:1	17
	2.54	6:1	19
3.2	1.00	—	—
	2.54	—	—
7.6-cm-dia Horn Lens Antenna			
7.6	1.00	62:1	35
	2.54	61:1	39
	6.35	63:1	44
3.2	1.00	1.6:1	18
	2.54	3.8:1	22
	6.35	30:1	27

The 6.35-cm array signal intensity with the large antenna and 3.2-cm plate is about 6 dB higher than the 2.54-cm array. A signal minimum occurs at ~every 2 degrees of array revolution about a central vertical axis. The S/N ratio at this minimum was ~10:1. However, zero-signal nulls were observed when the beam was swept across the 6.35-cm array by horizontally rotating the 3.2- and 5.1-cm reflector plates. The areas between the effective retroreflecting areas of the 6.35-cm corners is comparable to the beam area. The nulls result when the beam is incident upon the nonretroreflective areas.

Images with human body backgrounds and various system parameters are shown in Figures 20 through 22. Figure 20(a) is a full field-of-view human image extending vertically from near head-top to the waist at center frame, and extending horizontally elbow-to-elbow. The head, neck, shoulders, upper arms, hands hooked in pockets, and sternum are visible. The 3.2-cm plate is indistinguishable from the sternum; its S/N = 1. Body side and back views in (b) and (c) have higher background signals yielding lower S/N ratios. Body rib and shoulder bone curved areas produce the highest background noise. These results illustrate the primary difficulty with smaller targets and the retroreflection system.

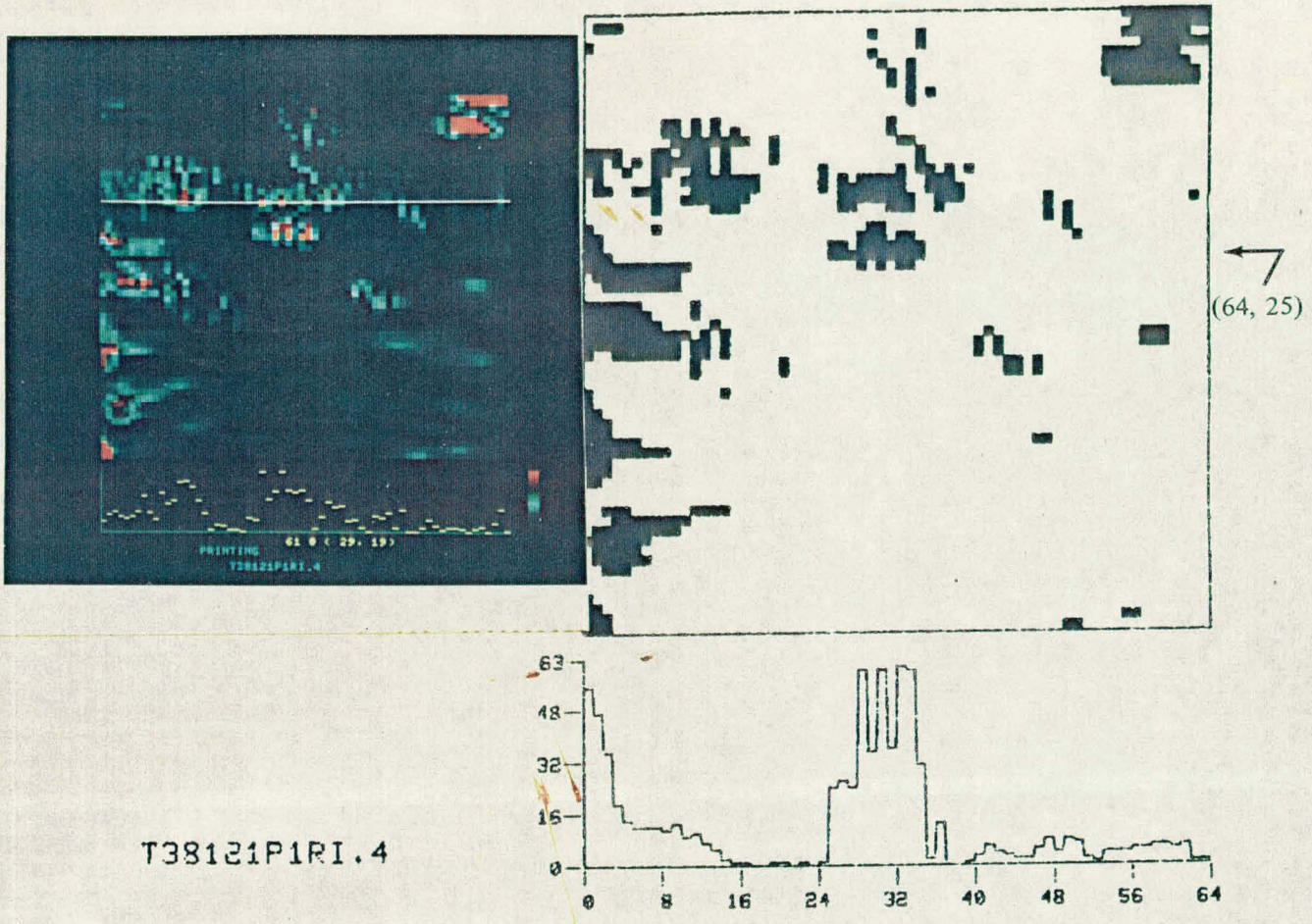

(a) Full Field-of-View Image, Human Body Front View, 19-dB Attenuation, S/N = 1

Figure 20. Radiometric Results, 7.6-cm-Diameter Horn/Lens Antenna, 3.2-cm Target Plate, 2.54-cm Retroreflector Array, Human Body Background

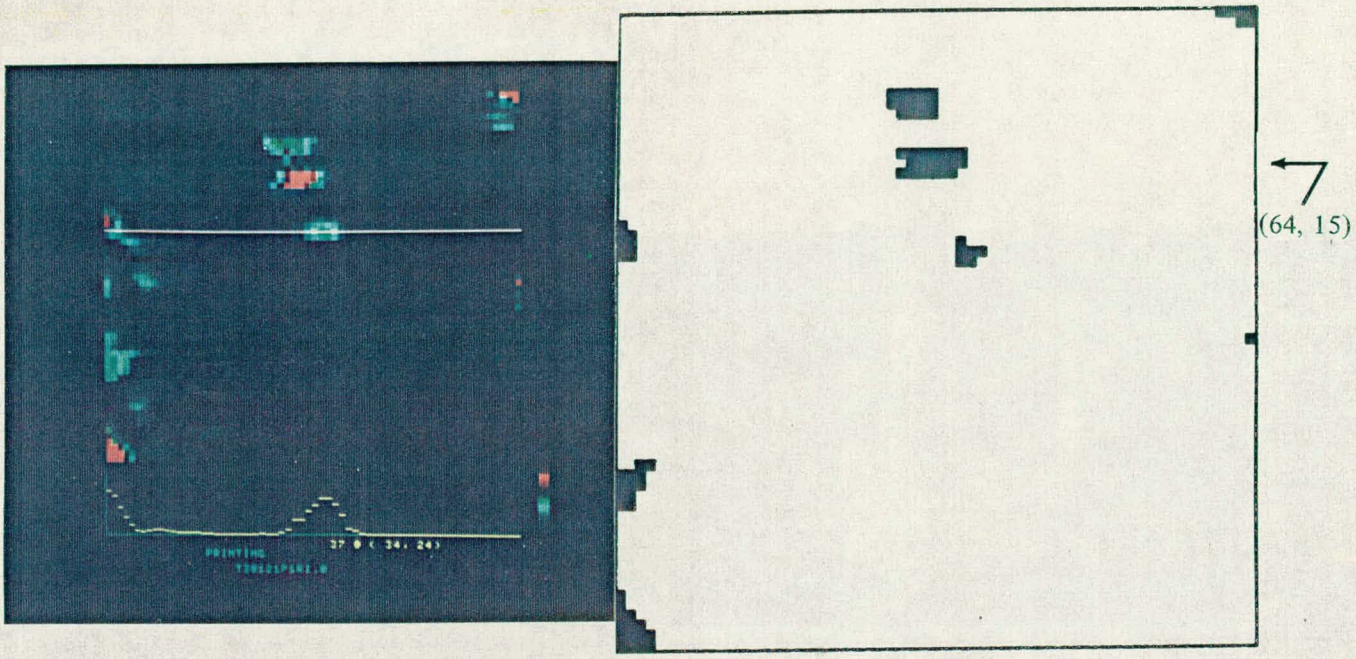

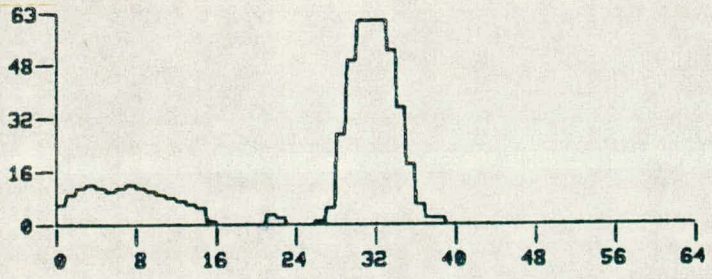

T38121P1RI.8

THE DATA VALUES IN THE HORIZONTAL SLICE BEGINNING AT (0, 15) ARE:

6	9	11	12	11	10	11	12	11	10	9	8	7	6	5	1
0	0	0	0	0	3	2	0	0	0	1	5	27	49	61	61
61	52	35	18	6	2	2	0	0	0	0	0	0	0	0	0
0	0	0	0	0	0	0	0	0	0	0	0	0	0	0	0

(b) Zoomed Image, Body Side View, 22-dB Attenuation, S/N = 0.61

PLOT IMAGE ? (1=YES,0=NO) 1
ENTER MINIMUM GRAY SCALE TO BE PLOTTED 31

Figure 20. (Continued)

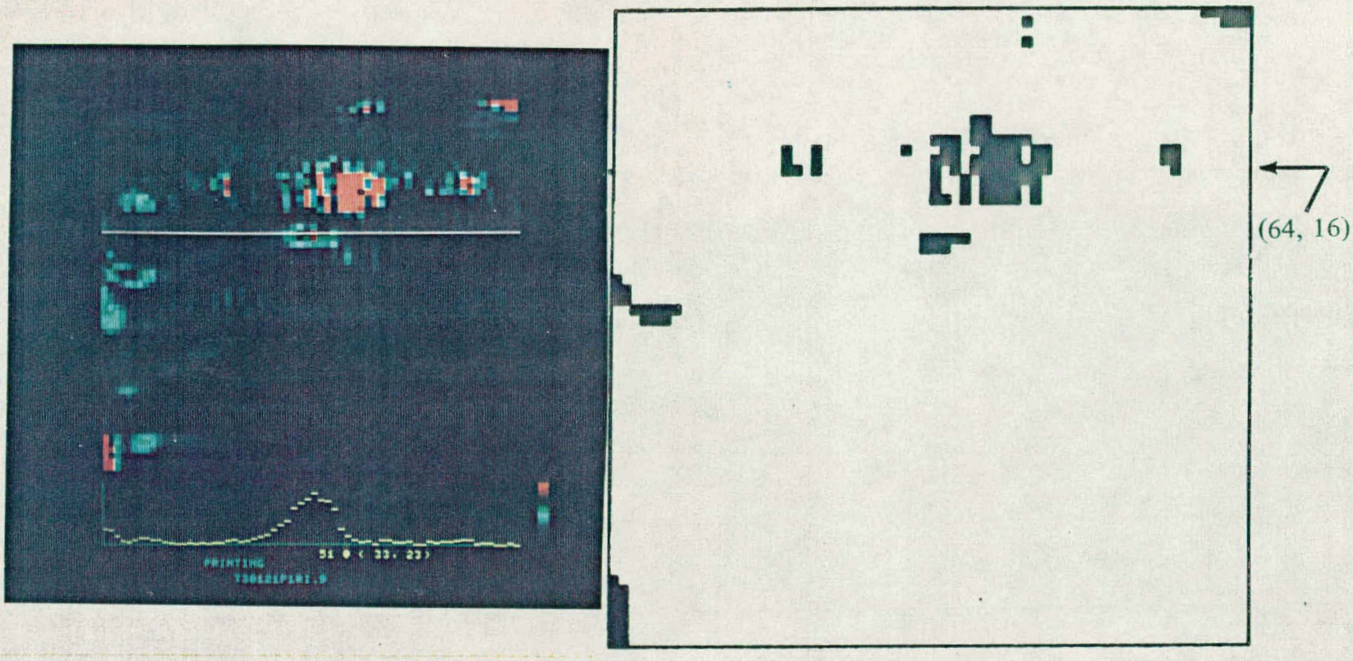

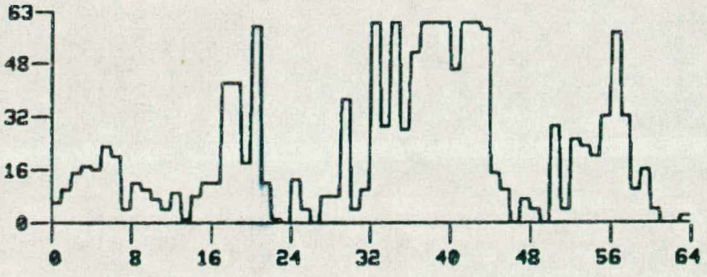

T38121P1RI.9

THE DATA VALUES IN THE HORIZONTAL SLICE BEGINNING AT (0, 16) ARE:

```
  6 10 15 17 16 23 20  4 12 10  7  4  9  1  8 12
 12 42 42 18 59 12  1  0 13  4  0  8  8 37  4 10
 60 29 60 28 51 60 60 60 46 60 60 58 15 10  0  7
  4  0 29  4 25 23 20 32 57 32 10 16  4  0  0  2
```

(c) Zoomed Image, Body Back View, 22-dB Attenuation, S/N = 0.85

```
PLOT IMAGE ? (1=YES,0=NO) 1
ENTER MINIMUM GRAY SCALE TO BE PLOTTED 39
```

Figure 20. (Concluded)

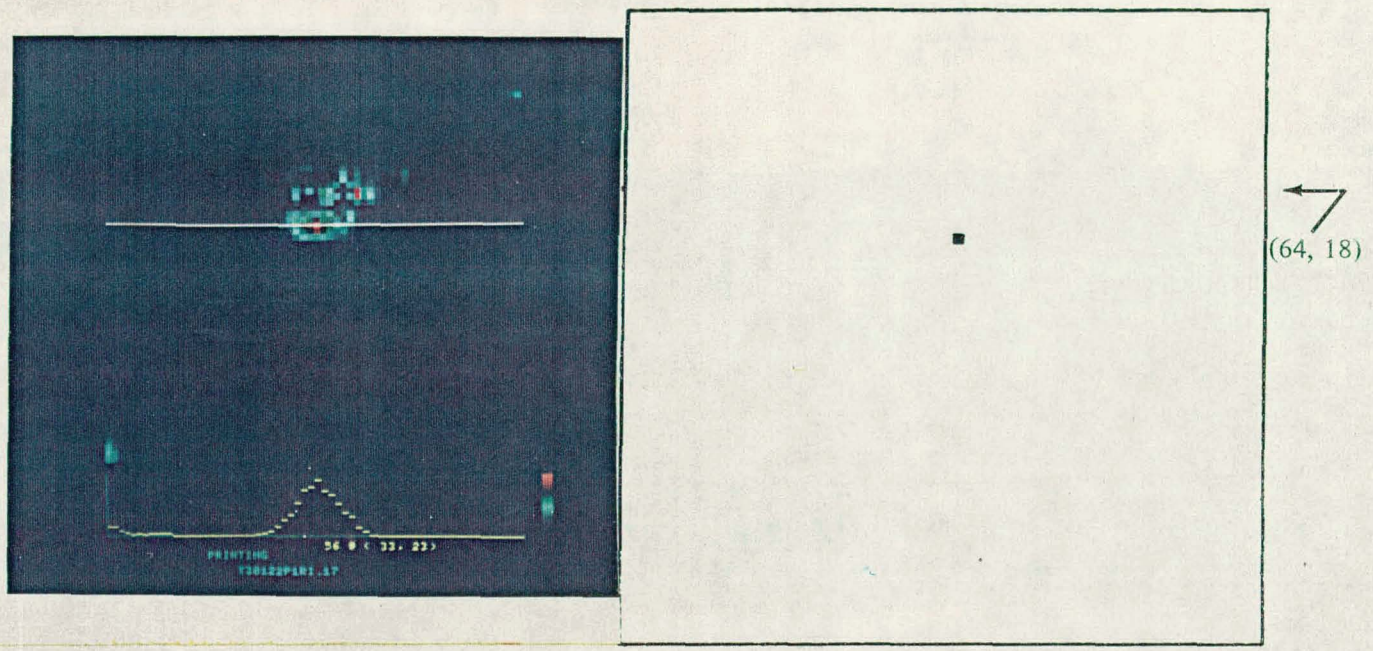

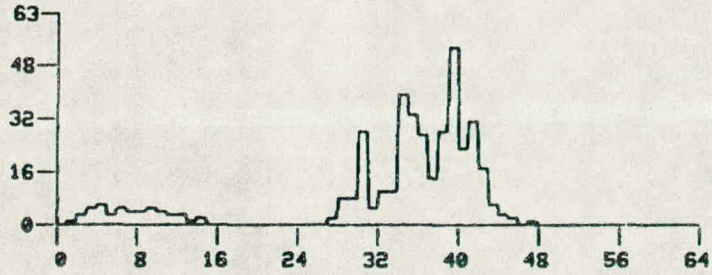

T38122P1RI.17

THE DATA VALUES IN THE HORIZONTAL SLICE BEGINNING AT (0, 18) ARE:

0	1	3	5	6	3	5	4	4	5	4	3	3	1	2	0
0	0	0	0	0	0	0	0	0	0	0	2	8	8	28	5
10	10	39	33	27	14	28	53	23	31	17	6	3	2	0	1
0	0	0	0	0	0	0	0	0	0	0	0	0	0	0	0

(a) 5.1-cm Target Plate, 28.5-dB Attenuation, S/N = 1:1

PLOT IMAGE ? (1=YES,0=NO) 1
ENTER MINIMUM GRAY SCALE TO BE PLOTTED 54

Figure 21. Radiometric Results, 7.6-cm-Diameter Horn/Lens Antenna, 2.54-cm Retroreflector Array, Human Body Background, Back View

THIS PAGE

WAS INTENTIONALLY

LEFT BLANK

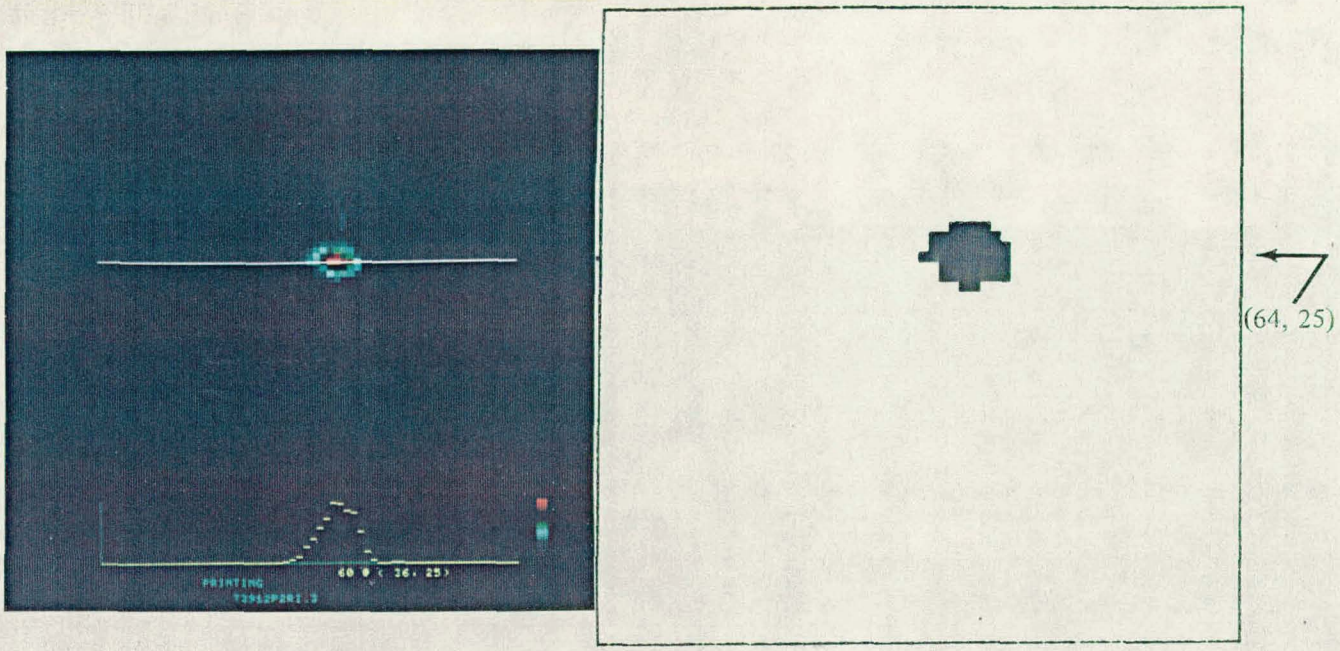

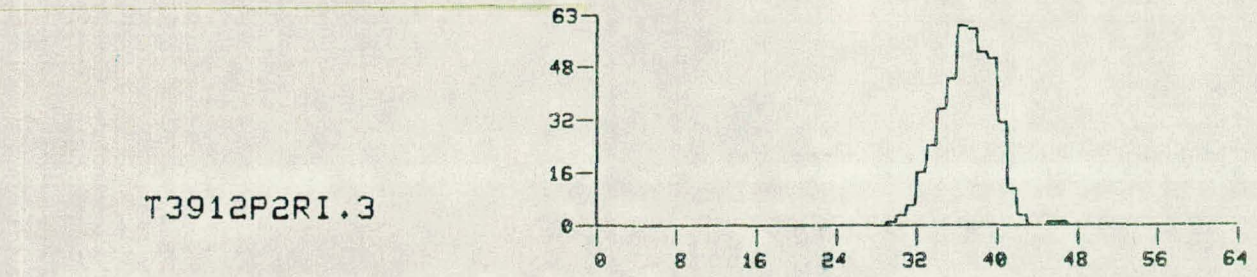

T3912P2RI.3

THE DATA VALUES IN THE HORIZONTAL SLICE BEGINNING AT (0, 25) ARE:

```
 0  0  0  0  0  0  0  0  0  0  0  0  0  0  0  0
 0  0  0  0  0  0  0  0  0  0  0  0  0  1  3  6
16 24 35 44 60 59 52 50 31 11  3  0  0  1  1  0
 0  0  0  0  0  0  0  0  0  0  0  0  0  0  0  0
```

5.1-cm Target Plate, 33.8-dB Attenuation, S/N = 4.0

PLOT IMAGE ? (1=YES,0=NO) 1
ENTER MINIMUM GRAY SCALE TO BE PLOTTED 15

Figure 22. Radiometric Results, 7.6-cm-Diameter Horn/Lens Antenna, 6.35-cm Retroreflector Array, Human Body, Back View

Body back-view (worst-case) examples with 5.1- and 7.6-cm plates and the 2.54-cm array are shown in Figure 21. The 5.1-cm plate S/N ratios were about 1:1, 2.5:1, and 6:1 for the back, side, and front views, respectively. The 7.6-cm-plate S/N ratios were about 18:1 and 26:1 for back and front views, respectively. These results denote the probable target size detection limits of this method.

Figure 22 is a body back view with the 5.1-cm plate and the 6.35-cm retroreflector array yielding a S/N ratio of 4.0. The body front view and side view S/N ratios were 20 and 12, respectively. The S/N ratio was 1.5 for the 3.2-cm plate and body front view. These 6.3-cm retroreflector results are included to note the improved signal although the aforementioned dead areas probably preclude its use.

The 25.4-cm diagonal hexagon array (Figure 8e) composed of 2.54-cm triangular corners was designed for test and assembly into more complete, all-angle, reflecting wall areas. An aluminum mold was constructed and arrays fabricated of filled epoxy and gel coat surfaced with conductive silver paint. Compared with the 2.54-cm retangular array, this array is 4.6 times larger in area with no exposed corner edges and produced a reflected beam approximately 1.7 times higher in intensity. S/N ratios for the triangular hexagon array and the rectangular arrays with a 5.1-cm plate and Eccosorb background were 54:1 and 20:1, respectively, indicating improved operation with the larger hexagon array.

Results against a body background are summarized in Table 2. The 7.6-cm antenna was used throughout.

Direct Backscatter and "Lost-Beam" Methods

Workable results were not obtained with the direct backscatter or the "lost beam" method, i.e., returns from unaligned plates were of insufficient contrast with the background for reliable detection. Direct backscatter from unaligned plates was not observed at ordinary beam power levels.

In the "lost beam" method at high power levels, the interference effects from radiation backscattered by the scanning mirror system obscured any indication of the body background or target. A 15- x 20-cm plate, which encompasses a number of fringes in the image, produced the "lost beam" effect at a moderate beam intensity, but once again at a low S/N ratio of ~1. A typical image is shown in Figure 23. Direct scanning with the hybrid tee radiometer or the use of a Dicke system may reduce interference effects. However, this method is not practical because curved areas of the body at an angle to the incident beam will also reflect the illumination away from the detector and appear dark at reasonable beam intensities.

Table 2. Radiometric Results Against a Body Background

Target Plate (cm)	Body Background View	S/N Ratio	Attenuation (dB)
2.54-cm Retroreflector Array			
7.6	Front	26:1	39
5.1	Back	18:1	39
5.1	Front	6:1	28
	Side	25:1	28
	Back	1:1	28
3.2	Front	1:1	19
	Side	0.6:1	22
	Back	0.9:1	22
6.35-cm Retroreflector Array			
5.1	Front	20:1	34
	Side	12:1	34
	Back	4:1	34
2.54-cm Hexagonal Array			
5.1	Eccosorb	54:1	31

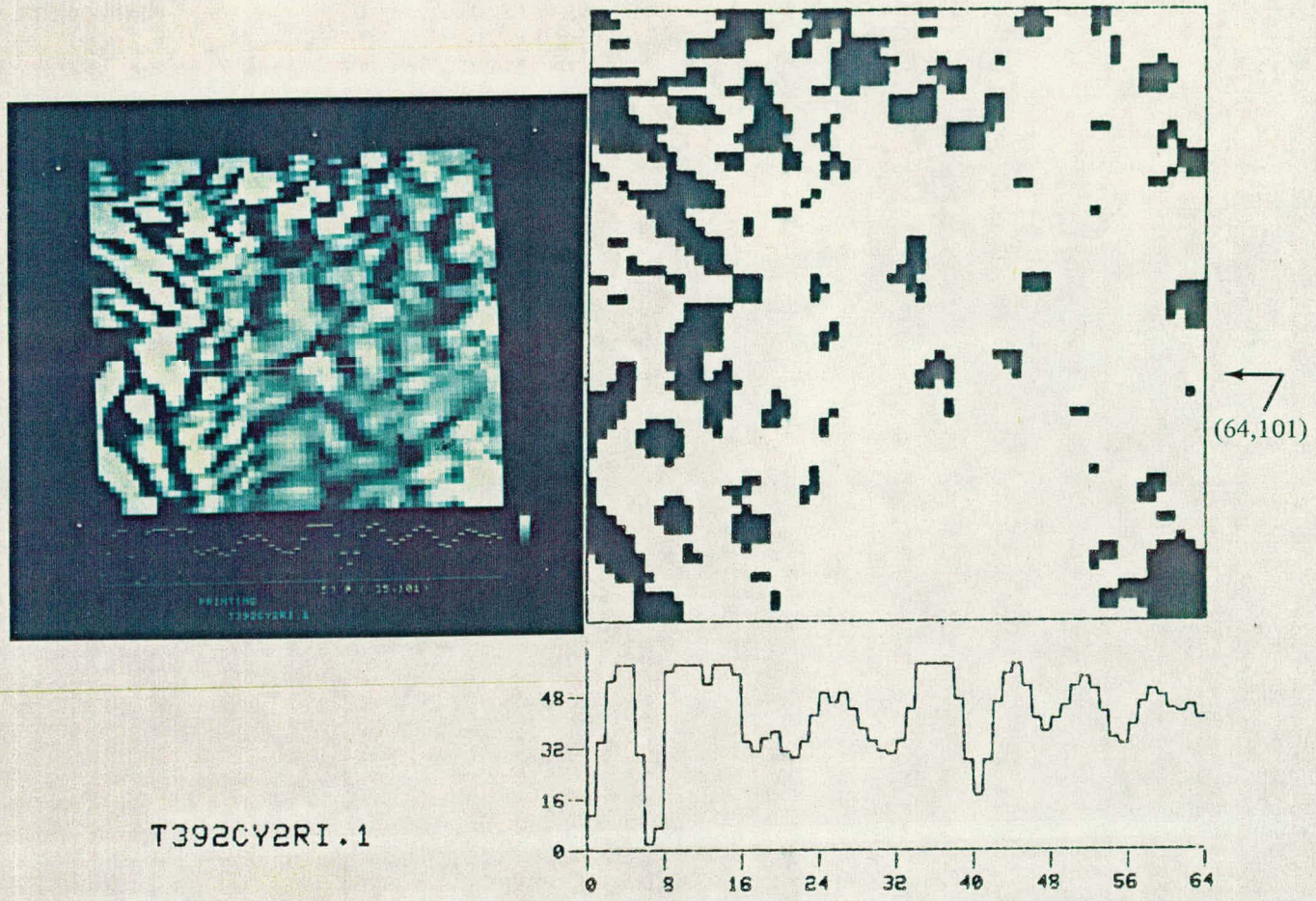

THE DATA VALUES IN THE HORIZONTAL SLICE BEGINNING AT (0,101) ARE:

```
11 34 53 58 58 30  2  7 56 58 58 58 52 58 58 55
34 31 35 37 31 29 34 42 49 46 49 44 38 34 31 30
34 44 58 58 58 58 47 28 17 28 46 55 58 51 41 37
41 45 51 54 50 43 35 33 39 46 50 48 44 43 45 41
```

1.8-cm-dia x 5-cm Metal Cylinder, 17.6-dB Attenuation, S/N = 1

```
PLOT IMAGE ? (1=YES,0=NO) 1
ENTER MINIMUM GRAY SCALE TO BE PLOTTED 57
```

Figure 23. Radiometric Results, "Lost Beam" Method, Body Background

Polarized Radiation

The use of wire-grid polarizers was briefly investigated in an attempt to distinguish the retroreflected target signal return from the directly reflected body background signals for target detection.* Both plane and circularly polarized radiation were employed using double wire-grid polarizers described in Appendix B. Also, see Figure 12(c) and (d). Circularly polarized radiation is reversed upon reflection, and a retroreflected beam, having undergone an odd number of reflections, will not be transmitted back through the same grid system into the detector. However, in this case, the retroreflected beam undergoes an additional even number of reflections compared with the body background reflected beam, both beams arrive similarly polarized at the detector, and no distinction can be expected by virtue of this process. Both the plane and circularly polarized results, including S/N ratios, were nearly identical to the original data and did not distinguish between signals.

Conclusions

The following conclusions and discussions were drawn from the retroreflection/hybrid tee radiometer investigations carried out at SNL during FY81. The FY81 period was the time allotted to assess the possible development of a practical NMMW personnel search system. Our studies are not considered exhaustive and it is felt that further development, if desired, might produce a method for use in highly specific, controlled search situations.

1. A refined hybrid tee, retroreflective, flying-spot system can possibly be made to "work"** with a horn/lens antenna of ~7.6-cm dia for the detection of flat metal plate targets ≥ 25 cm^2. However, fabrication of an all-angle, retroreflector illuminator enclosure with direct scanning and body rotations was not completed within the experimental time-frame and thus did not verify this conclusion or the detection of irregular, cylindrical, or spherical targets.
   a. Targets of smaller area are obscured by the directly reflected body background noise. The S/N ratio is ~1:1 for smaller targets.
   b. The reflection and retroreflection process, at 3 mm as developed here, introduces an attenuation of ~20 dB in the signal return of smaller area target plates. This attenuation reduces the small metal target signal (100% reflectivity) to approximately equal the direct body background signal (1% to 2% reflectivity) and limits the target size detection capability of this method.
2. An all-angle illumination source would not require the retroreflection process and would retain the 50 to 100:1 contrast ratio between a metallic target and body background. However, a practical source of this type is not available.
   a. An all-angle source can be constructed with a sufficient number of FIR sources, power dividers, and horns, but the cost is prohibitive.
   b. The LN_2 cold wall is considered attainable but unsatisfactory for maintenance and moderate signal increase reasons.
   c. Further development is required for detection of small, irregular, and/or low reflectivity targets by this approach.
3. The direct backscatter (glint) method was unsuccessful and would be effective only for targets of irregular shape which have sufficiently large surface areas that reflect back into the detector. The present method will not reliably detect a randomly oriented 0.38 caliber revolver or ordinary quantities of shielding or explosive materials against a human body background.
4. The "lost beam" method was not successful. This method is basically not feasible because the entire cross section of curved, specularly reflecting body parts cannot be saturated at reasonable illumination levels. The body areas at larger incidence angles to the beam also appear dark and do not provide a suitable background for detection.

*Molectron Corp., ITT North Wolfe Road, Sunnyvale, CA 94086

**"Work" is defined as: ~90% detection probability; 5% false alarm rate; 30- to 60-s search period with control of subject position and reflective articles carried in clothing; and an estimated cost in 5 yr of $75K in 1981 dollars. The low probability of detecting targets obscured in inaccessible body areas and crevices is neglected.

a. Target reflections were indistinguishable from body background with intense illumination.

b. Body background reflections were not uniform under intense illumination. High scattered radiation levels from the mirror system tend to obscure target reflections and introduce diffraction effects.

c. A region of sufficient target/background contrast was not found at lower illumination levels.

5. Reducing the radiation wavelength to 1.4 mm (215 GHz) will increase system resolution and improve retroreflector efficiency at this shorter wavelength. Unfortunately, equipment at this frequency is less available and much more costly.

6. Other possible detection and system improvements are: further signal processing, contiguous pixel requirements for detection, and direct scanning. It is unlikely however, that these improvements will counter the fundamentally low S/N ratio of the retroreflection method or the all-angle illumination problems.

7. Further development of increased optical collection scanning systems may be fruitful, both to reduce search time in the passive mode and to increase the ratio of detector area to illuminating beam area in a flying-spot bistatic, active method.

8. An overall appraisal of the FIR detection project indicates that a practical system, both in operation and cost at the present state-of-the-art, would require considerably more development and time without assurance of success. Given this developmental status and the perceived low user acceptance for a system of this type, a decision was made to discontinue the program at this time.

APPENDIX A

Previous Results

1. Transmission and Reflection Properties of Some Pertinent Materials

Typical transmission at 1.4-cm and 3-mm is ~95% for thin clothing, 85% and 90% respectively for demin, and 40% and 70% for 2.4-mm-thick leather. Data for many pertinent materials are given in References 1-8.

The reflectivity of human tissue is ~1.5% and metal is nearly 100%. Reflection investigations at 0.44- and 1.22-mm wavelengths indicated values of ~1.6% and 1.2%, respectively, for the surface of a human hand. Detasheet, TNT, and C-4 were 8.0%, 6.4%, and 3.7%, respectively, at 0.44 mm and 3.9%, 5.2%, and 0.95% at 1.22 mm (the irregular C-4 patty scattered strongly). Stick dynamite and ammonium nitrate tube reflectivity, a function of the container, was ≤1.5%. Later measurements of water gel dynamites, Atlas Aquafloe, Powermax 100, and Apex 700 at 1.4 and 3 mm gave reflectivities of 10% and 20%, respectively; the same results were obtained for water in a styrofoam container.

2. Passive Mode Detection Limitations

The scanning radiometer mirror system produces images at a scan rate of 1.5 s/line or a frame period of 75 s for a 1-m^2 raster. This period is considered excessive for most applications. Also, the passive signal level is not sufficient to allow an increase in scan rate because the maximum signal ΔT obtainable (for metal) is only ~10K which is the difference between body emission temperature and reflected ambient temperature. In addition, the observed variation in body background is 2 to 3K, which makes it virtually impossible to reliably detect explosives (or any other material with emissivity similar to the body) in the passive mode within the body background temperature variations.

3. Active Mode Illumination Parameters

Cold Source

Metal plates, several cm^2 in area, were detected with a signal to noise ratio of ~20:1 using the incomplete cold source. The source consisted of two LN_2 cooled boxes, 1 x 0.6 x 0.2 m in size and a few smaller ones to fill some of the gaps around the mirror scanning system. The source emission temperature (77 K) is reflected from the metal object against the human body (304 K) and produces a radiometric difference signal ΔT of ~227 K.

Klystron Illumination

Coherent klystron illumination was employed at 1.4- and 3-mm wavelengths. A 10-μW beam from a horn antenna illuminated a 20-cm-dia target area (half-power beam width at the focal plane of the scanning system). Appropriate metal objects produce high contrast signals (S/N ratio >50). System resolution was observably better at 1.4 mm, the shorter wavelength. However, the 3-mm detector is more sensitive by a factor of 3 and the water-based explosives reflectivity is doubled at this wavelength. The choice of wavelength will depend on specific requirements. Composite nuclear shielding was detected with relatively high contrast against Eccosorb at both wavelengths. There was slightly less contrast against the human body, about 2:1.

APPENDIX B

Quasi-Optical System Components

In the near-millimeter-wave region, microwave and optical design methods blend into a hybrid approach called "quasi-optics" which uses the best of both methods to optimize the performance of microwave and optical components.[12-19] Various quasi-optical components (shown in Figure 12 in the main text of this paper) were used in preliminary experiments with the apparatus shown in Figure B-1 prior to the delivery of hybrid tee radiometer components and assembly of the scanning system. A near-on-axis Cassegrain Dicke radiometer-illuminator system is seen at the right of the photograph. Centered in front of the Cassegrain collector optics is an illuminator beam waveguide source fed by a Gunn diode oscillator and a beam collimating teflon lens. A metal plate target is mounted at photo left and a single 6.35-cm retroreflector is seen next to the Cassegrain tube. Single-dimension scanning was accomplished by linear sample movement. Initial reflection data and detection experiments were performed and later corroborated by the hybrid tee interferometer-radiometer scanning system. Double prism and wire-grid beam splitters were also employed in front of the Cassegrain collector to position the illuminator beam on-axis for retroreflection purposes. These, however, produced increased scattering and diffraction problems compared with the horn/lens antenna in the configuration shown.

Collimated Horn/Lens Antenna

The 2.54-cm-dia horn/lens, collimated beam antenna (see Figure 12(a) in the main text and Figure B-2 in this Appendix) was designed by these methods.[16-22] The optimum horn electrical length is given by

$$\frac{L}{\lambda} = 0.3\left(\frac{D}{\lambda}\right)^2 \quad ,$$

where

L is conical horn slant length and D is aperture diameter.

The inside surfaces of the horn are corrugated. The corrugation alters the surface reactance to suppress higher order modes of excitation and backlobes, and provides circularly symmetric, low sidelobe patterns for illuminating lens and reflectors.[22]

The reactance X of the surface is

$$X = \frac{g}{g+t}\sqrt{\frac{\mu}{E}}\tan k_o d \quad ,$$

provided that $g/(g+L) \approx 1$ which is satisfied if $L \leq g/10$. The slot width g must also be small compared to both the wavelength and the slot depth d. For $g \leq \lambda/10$, $\lambda/4 < d < \lambda/2$. These requirements were relaxed ($g = \lambda/8$) to facilitate machining. The 2.54-cm-dia plano-convex collimating lens was designed by the lens equation

$$r = \frac{f(n-1)}{n\cos\theta - 1} \quad ,$$

where r is focal point-lens distance, f is focal length, and n is the refractive index of rexolite (1.59). The quarter-wave, antireflection corrugated surface was machined into the plane surface using the data of Morita and Cohn.[23] This matches the free air and lens material to cancel surface reflections and reduce back and side lobes and improve the antenna gain. A match may be obtained at the desired frequency and incidence angle by adjusting the groove depth and width. A compromise width dimension (0.81 mm) between those calculated for horizontal and vertical grooves, relative to the E field, was used for the circular, concentric horn/lens corrugation. The parallel grooves in the prism and lens (Figure 12(d) and (e) in the text) are 0.97 mm. The corrugation "teeth" are 0.42 mm wide and 0.518 mm high.

Double-Prism Beam Splitter

The dielectric double prism (see Figure 12(b) of the text) is a quasi-optical device which can function as a beam splitter, attenuator, or coupler.[13,24,25] These prisms were designed from data in the cited references

and machined from rexolite with 0.004-cm prism tolerances. The surfaces are grooved for antireflection purposes. The principles of total reflection for a wave incident on the interface between two dielectrics at an angle greater than the critical angle and frustrated reflection are used. The attenuation and off-axis coupling can be varied by changing the prism separation along the diagonal. With no gap, the beam is transmitted; with a single prism, the beam is totally reflected at 90°. With a gap between the prisms, the beam is partially transmitted and partially reflected. Thus, the splitting ratio can be adjusted by varying the gap separation.

Parallel Metallic Wire Grid Beam Splitter and Polarizer

Parallel wire grids are almost completely transparent for radiation polarized with the electric vector perpendicular to the wires. Parallel polarized radiation is partially transmitted and partially reflected. A grid functions as a beam splitter when inserted into a polarized beam at an angle of 45° and rotated to vary the ratio of transmitted-to-reflected (90°) radiation. A plane polarized beam can be circularly polarized by a grid positioned normal to the beam and rotated 45° to the plane of polarization.

A 6-cm-dia wire grid of the text, larger than the commercially available one (Figures 12(c) and (d) of the text), was constructed as described by Sentz.[26] Grid theory is given by Marcuvitz[14] and the design followed the analyses of Ulrich.[27-29] For a one-dimensional parallel wire, capacitive grid, and nearly normal incident radiation, the grating constant (distance between wire centers g) must be smaller than the wavelength λ to avoid diffraction sidewaves. For $\lambda \gg g$, the complex reflection coefficient R of an equivalent electrical circuit is

$$R = -\frac{Y/2}{1+Y/2}$$

and the transmission coefficient is

$$T = 1 + R \ ,$$

where Y is the characteristic admittance.

For circular wires of radius a,

$$Y = -j\left(\frac{2\lambda}{Z_o g}\right) \text{ and } Z_o = \frac{1}{\ln(g/2\pi a)} \ .$$

Grid parameters were a = 64 μm and g = 500 μm.

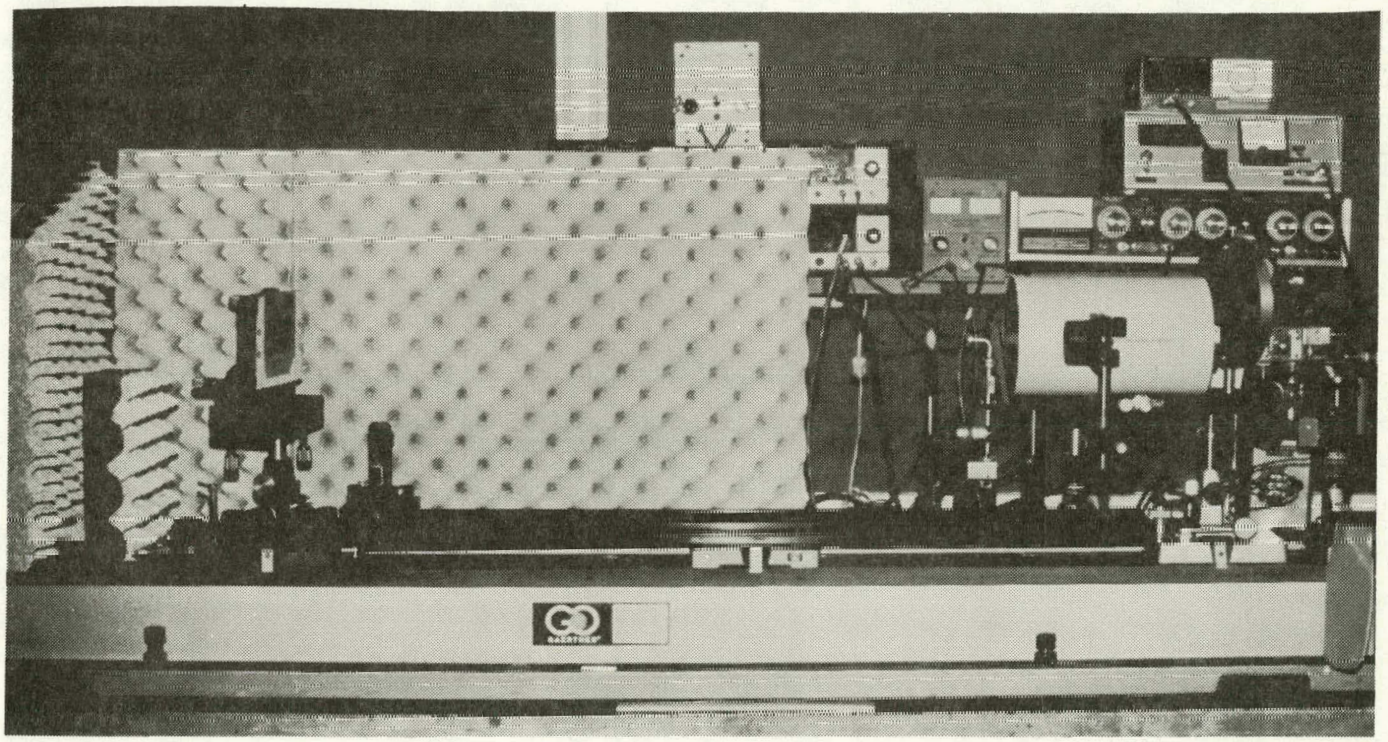

Figure B-1. Nonscanning Cassegrain Dicke Radiometer/Illuminator Experimental System

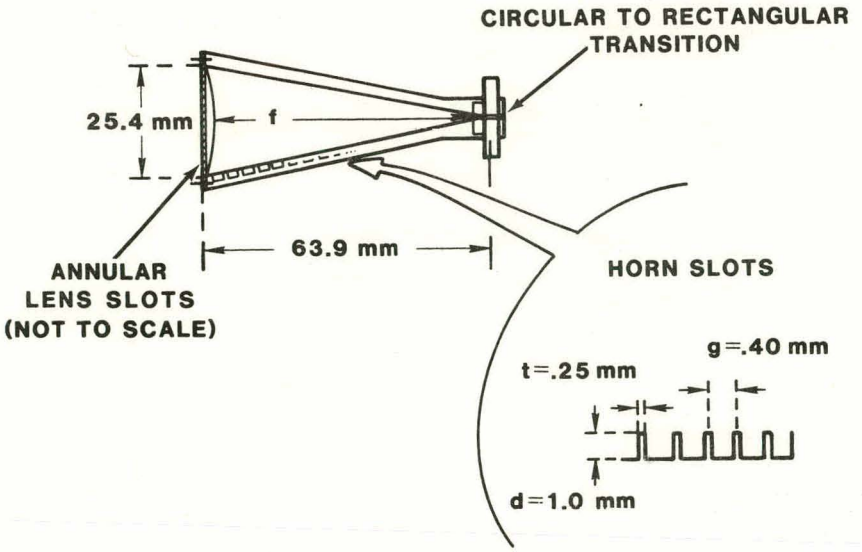

Figure B-2. 2.54-cm-Diameter Conical, Collimated Horn/Lens Antenna

References

[1]D. T. Hodges, F. B. Foote, and R. D. Reel, *Feasibility of FIR Detection of Selected Materials*, report prepared for Sandia National Laboratories, Aerospace Report No. ATR-77(7675)-1, The Aerospace Corporation, September 30, 1977.

[2]E. E. Rebes, F. B. Foote, D. T. Hodges, The Aerospace Corporation, and R. L. Schellenbaum, SNL, *Evaluation of Passive Far-Infrared Radiometric Techniques for Detection of Concealed Objects*, SAND80-1263 (Albuquerque: Sandia National Laboratories, 1980).

[3]D. T. Hodges, E. E. Reber, and F. B. Foote, The Aerospace Corporation, and R. L. Schellenbaum, SNL, *Safeguards Applications of Far-Infrared Radiometric Techniques for the Detection of Contraband*, SAND79-7081 (Albuquerque: Sandia National Laboratories, 1980) and *Jour Inst Nuc Mat Mgt* IX:1, Spring 1980.

[4]D. T. Hodges and E. E. Reber, *Evaluation of Passive Far-Infrared Radiometric Techniques for Detection of Concealed Objects*, final report prepared for Sandia National Laboratories, Aerospace Report ATR-79(7745)-1, The Aerospace Corporation, March 23, 1979.

[5]M. Scotto, *The Use of Far-Infrared Radiation for the Detection of Concealed Metal Objects*, DOT-TSC-OST-72-119 (Washington, DC: Department of US Transportation, 1971).

[6]F. D. Colegrove et al, *Image Crowd Surveillance System U1-84-150-F*, final technical report for US Army Mobility Equipment Research and Development Center (Dallas,TX: Texas Instruments, Inc, 1973).

[7]D. H. Barker, D. T. Hodges, and T. S. Hartwick, "Far-Infrared Imagery," *SPIE J* 67:27-34, 1975

[8]T. S. Hartwick et al, "Far-Infrared Imagery," *Appl Opt* 15:1919-1921, 1976.

[9]R. M. Weigand, *A Microwave Technique for Detecting and Locating Concealed Weapons*, DOT-TSC-OST-72-16 (Washington, DC: US Department of Transportation, December 1971).

[10]R. C. Spencer, *Optical Theory of the Corner Reflector*, MIT RL-433 (Cambridge: Massachusetts Institute of Technology, March 2, 1944).

[11]Henry Jasik, Ed., *Antenna Engineering Handbook* (New York: McGraw-Hill, 1961).

[12]J. Gallagher, "Optics in the Far Infrared," *Electro-Optical Systems Design*, November 1980, pp 25-31.

[13]J. H. Rainwater and R. W. McMillan, "A Hybrid Technology for Near-Millimeter Waves" *Microwaves*, June 1980, pp 76-82.

[14]N. Marcuvitz, *Waveguide Handbook, MIT Radiation Laboratory Series* (New York: McGraw-Hill, 1951).

[15]H. Jasik, *Antenna Engineering Handbook* (New York: McGraw-Hill, 1961).

[16]S. Silver, *Microwave Antenna Theory and Design* (New York: McGraw-Hill, 1949).

[17]E. A. Wolff, *Antenna Analysis*, (New York: Wiley, 1966).

[18]T. Milligan, "Universal Patterns Ease Circular Horn Design," *Microwaves*, March 1981, pp 83-86.

[19]G. R. Loefer et al, "Computer Analysis Speeds Corrugated Horn Design," *Microwaves*, May 1976, pp 58-65.

[20]J. Brown, *Microwave Lens* (John Wiley & Sons, Inc, 1953).

[21]R. Tremblay and A. Boivin, "Concepts and Techniques of Microwave Optics," *Applied Optics* 5:2, February 1966.

[22]R. E. Lawrie and L. Peters, Jr., "Modifications of Horn Antennas for Low Sidelobe Levels," *IEEE Transactions on Antennas and Propagation* AP-14:5, September 1966.

[23]T. Morita and S. B. Cohn, "Microwave Lens Matching by Simulated Quarter-Wave Transformers," *Trans. IRE* AP-3, January 1956.

[24]J. J. Taub et al, "Submillimeter Components Using Oversize Quasi-Optical Waveguide," *IEEE Transactions on Microwave Theory and Techniques*, MTT-11, September 1963.

[25]R. G. Fellers, "Measurements in the Millimeter to Micron Range," *Proceedings of the IEEE* 55:6, June 1967.

[26]A. Sentz et al, "Construction of Parallel Grids Acting as Transparent Flat Mirrors in the Far Infrared," *Review of Scientific Instruments* 49:7, July 1978, pp 926-927.

[27]R. Ulrich, T. J. Bridges, and M. A. Pollack, "Variable Metal Mesh Coupler for Far Infrared Lasers," *Applied Optics*, 9:11, November 1970, pp 2511-2516.

[28]R. Ulrich, K. F. Renk, and L. Genzel, *IEEE Transactions* MTT-11:363, 1963, pp 363-371.

[29]R. Ulrich, "Far-Infrared Properties of Metallic Mesh and its Complimentary Structure," *Infrared Physics*, Vol. 7, Pergamon Press Ltd, 1967, pp 37-74.

Do Not
Microfilm Distr.

DISTRIBUTION:

US Department of Energy (2)
Office of Safeguards and Security
Washington, DC 20545
Attn: R. E. Caudle
G. A. Hammond

The Aerospace Corporation
2350 E. El Segundo Blvd
El Segundo, CA 90009
Attn: E. Danielwitz

9200 W. C. Myre
9210 V. E. Blake
9220 C. H. Mauney
9230 M. L. Kramm
9250 T. A. Sellers
9252 M. J. Eaton
9252 R. L. Schellenbaum (25)
9254 I. G. Waddoups
9260 J. Jacobs
9410 D. J. McCloskey
Attn: G. B. Varnado, 9414
L. D. Chapman, 9416
3151 B. J. Tolman
8214 M. A. Pound
3141 L. J. Erickson (5)
3151 W. L. Garner (3)
3154-3 C. H. Dalin (5)
For DOE/TIC
(Unlimited Release)

Org.	Bldg.	Name	Rec'd by	Org.	Bldg.	Name	Rec'd by

Sandia National Laboratories